JEM Journal of Experimental Medicine

ARTICLE

Suppression of ILC2 differentiation from committed T cell precursors by E protein transcription factors

Liangyue Qian[1], Sandra Bajana[1], Constantin Georgescu[1], Vincent Peng[2], Hong-Cheng Wang[1], Indra Adrianto[1,5], Marco Colonna[2], Jose Alberola-Ila[1,3], Jonathan D. Wren[1], and Xiao-Hong Sun[1,3,4]

Current models propose that group 2 innate lymphoid cells (ILC2s) are generated in the bone marrow. Here, we demonstrate that subsets of these cells can differentiate from multipotent progenitors and committed T cell precursors in the thymus, both in vivo and in vitro. These thymic ILC2s exit the thymus, circulate in the blood, and home to peripheral tissues. Ablation of E protein transcription factors greatly promotes the ILC fate while impairing B and T cell development. Consistently, a transcriptional network centered on the ZBTB16 transcription factor and IL-4 signaling pathway is highly up-regulated due to E protein deficiency. Our results show that ILC2 can still arise from what are normally considered to be committed T cell precursors, and that this alternative cell fate is restrained by high levels of E protein activity in these cells. Thymus-derived lung ILC2s of E protein–deficient mice show different transcriptomes, proliferative properties, and cytokine responses from wild-type counterparts, suggesting potentially distinct functions.

Introduction

Innate lymphoid cells (ILCs) are important contributors to protective immunity as well as to pathological conditions (Artis and Spits, 2015; Eberl et al., 2015). Therefore, the regulation of their homeostasis is of biological significance. Despite the lack of antigen receptors on their cell surface, three groups of ILCs, designated ILC1–3, exhibit parallel cytokine expression profiles and immune functions with the three subsets of T helper cells known as Th1, Th2, and Th17 (Spits et al., 2013; Robinette and Colonna, 2016). For example, like Th2 cells, ILC2s secrete IL-5 and IL-13. ILCs are considered first responders to various triggers upon pathogen infection, allergen exposure, and tissue damage (Tait Wojno and Artis, 2016).

Like B and T lymphoid cells, ILCs originate from lymphoid progenitors such as common lymphoid progenitors (CLPs) and lymphoid primed multipotent progenitors (LMPPs; Constantinides et al., 2014; Yang and Bhandoola, 2016; Zook and Kee, 2016). ILC differentiation has been shown to take place in the bone marrow (BM) through a series of precursors that descend from CLP or LMPP and gradually lose the potential to differentiate into B, T, or NK cells while maintaining the ability to generate ILC1, 2, and 3 (Constantinides et al., 2014; Klose et al., 2014; Yu et al., 2014, 2016; Yang et al., 2015). Since CLP and LMPP also seed the thymus and differentiate into T cells (Kondo et al., 1997; Balciunaite et al., 2005; Sambandam et al., 2005), the capacity of the thymus to support ILC development needs to be fully evaluated.

The basic helix-loop-helix transcription factors encoded by E2A, HEB, and E2-2 genes (also known as *Tcf3*, *Tcf12*, and *Tcf4*) are collectively called E proteins (Murre, 2005). E proteins are essential for the differentiation of both B and T cells immediately following their respective lineage commitment (Bain et al., 1994; Zhuang et al., 1994; Barndt et al., 2000). They also bias the multipotent progenitors toward the lymphoid fate (Dias et al., 2008; Cochrane et al., 2009). The functions of E proteins are impeded by a group of inhibitors called Id proteins (Sun, 1994; Kim et al., 1999; Wang et al., 2009; Ling et al., 2014). Id2 has been shown to be indispensable for ILC differentiation (Klose et al., 2014; Seillet et al., 2016). A role for E proteins in suppressing an innate lymphoid fate was first demonstrated in our Id1 transgenic mice, where Id1 is expressed under the control of the *lck* proximal promoter (Wang et al., 2017). In these mice, large numbers of phenotypic and functional ILC2s were generated in the thymus and distributed throughout the body, leading to heightened type 2 immune responses in allergy and parasite infection (Wang et al., 2017). In addition, specifically deleting the E2A and HEB genes in the thymus or in both the BM and thymus also resulted in marked increase in ILC2 production (Miyazaki

[1]Oklahoma Medical Research Foundation, Program in Arthritis and Clinical Immunology, Oklahoma City, OK; [2]Department of Pathology and Immunology, Washington University School of Medicine, St Louis, MO; [3]Department of Cell Biology, University of Oklahoma Health Sciences Center, Oklahoma City, OK; [4]Department of Microbiology and Immunology, University of Oklahoma Health Sciences Center, Oklahoma City, OK; [5]Department of Public Health Sciences, Henry Ford Health System, Detroit, MI.

Correspondence to Xiao-Hong Sun: sunx@omrf.org.

et al., 2017; Wang et al., 2017). Collectively, these data suggest that E proteins block the innate lymphoid fate not only in the BM but also in the thymus. However, whether the thymus normally contributes to ILC2 production in the body and at what developmental stages T cell precursors can divert to the ILC2 path are poorly understood.

In the current study, we took a number of in vivo and in vitro approaches to demonstrate a previously unappreciated capacity of committed T cell precursors ($CD4^-CD8^-$c-kit^-CD25^+ [DN3]) to differentiate into ILC2s in WT animals (Wong et al., 2012); these ILC2s exit the thymus to the periphery. Down-regulation of E proteins greatly enhances such a potential. As a result, peripheral tissues are populated with thymus-derived ILC2s, which are found to be hyperproliferative and have different sensitivities to ILC2 activators. Analyses of transcriptomes in the thymic ILC2s and cells at the early time points during in vitro ILC2 differentiation revealed a critical network of gene expression, primarily centered on the ZBTB16 transcription factor and IL-4 signaling pathway, which are repressed by E protein activities.

Results

tdTomato expression induced by the plck-Cre transgene marks thymus-derived ILC2 in the periphery

Previous studies showed that ectopic Id1 expression leads to massive overproduction of ILC2 (Wang et al., 2017), which is now confirmed to be dependent on the thymus, as crossing *plck-Id1* transgenic mice with athymic nude mice did not result in increases in ILC2 counts (Fig. S1 a). Whether this represents a natural function of the thymus remains unknown. To address this, we traced thymus-derived ILC2s using p*lck*-Cre; ROSA26-stop-tdTomato reporter mice, because the p*lck*-Cre transgene is found to be specifically turned on in the thymus, beginning at the $CD4^-CD8^-$c-kit^-CD25^+ (DN3) stage (Shi and Petrie, 2012; Wang et al., 2017). The p*lck*-Cre transgene did not cause tdTomato expression either in B and myeloid cells or in innate lymphoid progenitors and ILC2s in the BM (Wang et al., 2017). In contrast, tdTomato expression was detected in ∼30% of ILC2s in the thymus, suggesting that a fraction of ILC2s in the thymus differentiated from thymic progenitors, which already turned on the p*lck*-Cre transgene, or that these ILC2s expressed the transgene themselves (Fig. 1 a). Interestingly, we also observed a similar percentage of $tdTomato^+$ ILC2s in the blood, suggesting that thymic ILC2s exit the organ, circulate through the blood, and home to peripheral tissues. The generation of these $tdTomato^+$ ILC2s is dependent on the thymus, because significantly lower numbers of these cells were found in the blood of athymic nude recipients of p*lck*-Cre; ROSA26-stop-tdTomato BM progenitors compared with CD45.1 recipients (Fig. S1 b).

Of the peripheral tissues examined, we detected ∼10% of $tdTomato^+$ ILC2s in the lung. These lung $tdTomato^+$ ILC2s were unlikely to be contaminating blood ILC2s because intravenous injection of anti-CD45 antibodies shortly before harvesting lung cells did not mark ILC2s (data not shown; Huang et al., 2018). In contrast to the lung, few ILC2s in the white adipose tissue and small intestine were labeled with tdTomato, whereas 1–3% of ILC2s in the skin were $tdTomato^+$ (Fig. 1 a). Together, these results suggest that thymic ILC2s can populate the peripheral tissues through circulation, even though the possibility that ILC2s in peripheral tissues expressed the p*lck*-Cre transgene independently has not been ruled out.

We next generated p*lck*-Cre; ROSA26-stop-tdTomato; $E2A^{f/f}$; $HEB^{f/f}$ mice, in which Cre-mediated deletion resulted in E2A and HEB ablation and tdTomato expression. In these mice, >60% of thymic ILC2s were labeled by tdTomato (Fig. 1 b). Furthermore, the majority of ILC2s in other organs are also marked (Fig. 1 b). This is likely due to the massive output of ILC2s from the thymus, which resulted in >10-fold increases in ILC2 counts in different tissues (Fig. 1 c). Since *plck-Cre* is expressed largely after the DN3 stage (Wang et al., 2017), this raises the possibility that ILC2 differentiation can occur in committed T cell precursors such as DN3 cells and suggests that E proteins normally act to suppress the ILC2 potential in these T cell precursors.

Detection of TCRβ and TCRγ gene rearrangement in thymus-derived ILC2s

Taking advantage of the sequential events of TCR gene rearrangement during T cell development in the thymus (Mombaerts et al., 1992; Dudley et al., 1994), we measured TCR recombination events in ILC2s to assess the relationship between ILC2s and T cell precursors. We amplified representative rearranged TCR gene products using conventional PCR with primers binding to the V, D, or J regions of different TCR genes. ILC2s from different organs were sorted with extra efforts to eliminate T cell contaminations (Fig. S2 a). To facilitate semiquantitative estimation, we created standard curves by using cell mixtures of different proportions of BM $Mac1^+$ cells and total thymocytes (Fig. 2). BM ILC2s of WT mice had few TCR rearrangement events (Fig. 2, a and b). However, thymic ILC2s contained both Dβ2-Jβ2 and Vβ3-DJβ2 rearrangement of the TCRβ gene, and approximately half of the ILC2s had the TCRβ gene rearranged estimated based on the standard curves. The PCR product corresponding to the germline configuration was also detectable (Fig. 2 a). In addition, WT thymic ILC2s exhibited robust Vγ1-Jγ4 recombination (Fig. 2 b). The quantities of the DNA preparations were verified by PCR amplification of a fragment in the ROSA26 locus (Fig. 2 c).

Besides thymic ILC2s, ILC2s from the WT lung also displayed low levels of TCRβ and TCRγ gene rearrangement (Fig. 2, a and b), which is estimated to account for ∼5–10% of the level seen in total thymocytes. These rearrangement events were detected in lung ILC2s from $TCR\alpha^{-/-}$ but not nude mice (Fig. 2, a and b), thus indicating that events are thymus dependent and unlikely due to T cell contamination. These results suggest that a small fraction of lung ILC2s come from the thymus.

In contrast to WT ILC2s, the majority of ILC2s from the thymus and lung of the E2A and HEB double knockout mice (p*lck*-Cre; $E2A^{f/f}$; $HEB^{f/f}$ [dKO]) possessed the rearranged TCRβ, as the germline band of the TCRβ gene was undetectable (Fig. 2 a). TCRγ gene rearrangement was also readily detectable. These results suggest that ILC2s in the dKO mice are generated from committed T cell precursors such as DN3 cells, which already completed TCRβ and/or TCRγ gene rearrangements. These findings are consistent with the reporter analyses shown in

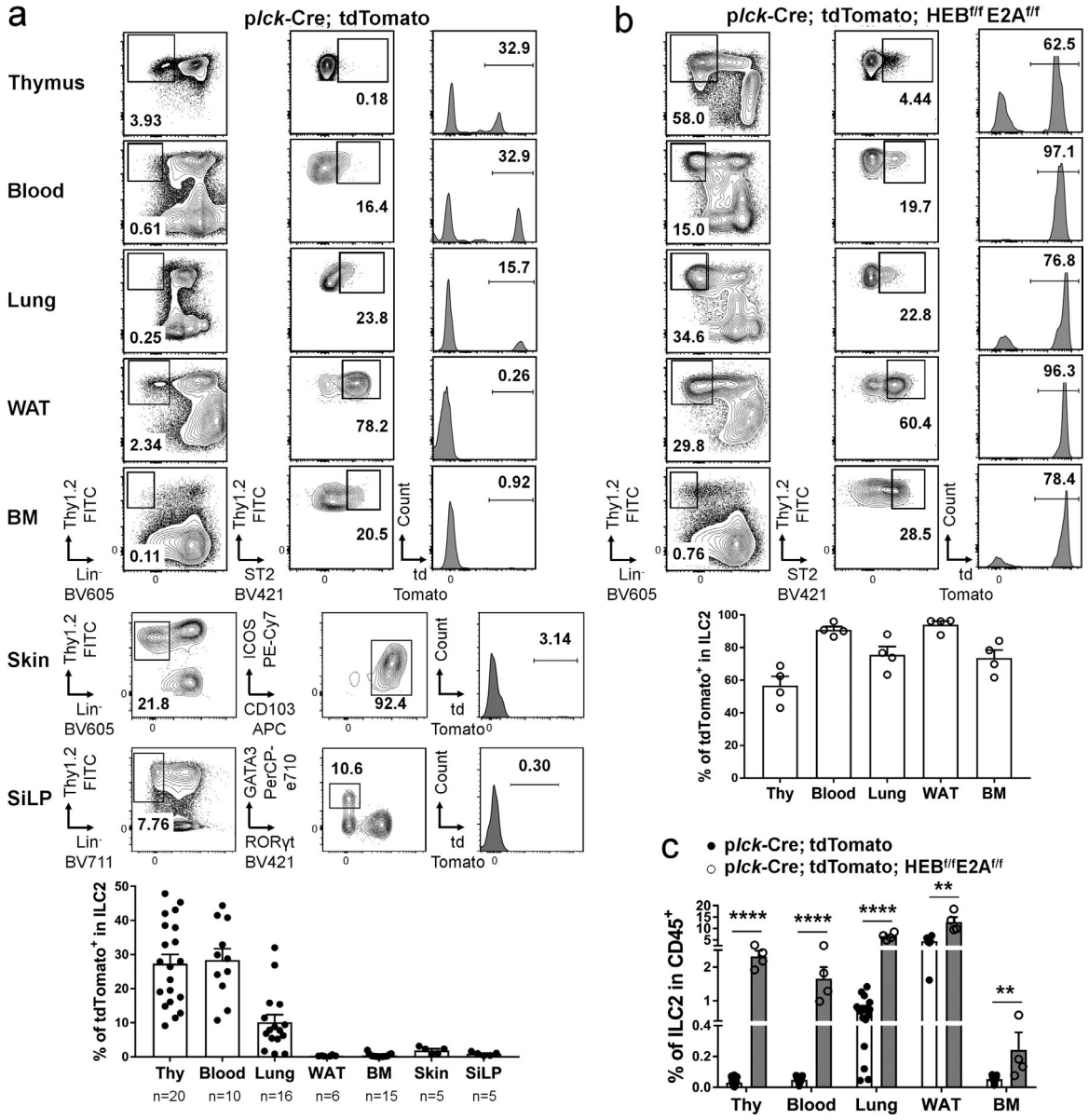

Figure 1. **Thymic ILC2s are traced with tdTomato expression induced by the *plck*-Cre transgene. (a)** Representative gating strategies for analyses of tdTomato expression in ILC2s from *plck*-Cre; ROSA26-stop-tdTomato reporter mice. Cells from indicated organs were stained for lineage markers together with antibodies against Thy1 and ST2 (except skin and small intestine). Live CD45$^+$ cells were gated before lineage analysis. To ensure the elimination of any contamination of T lineage cells, the Lin$^-$ population of each organ was further gated for TCRβ$^-$γδTCR$^-$ based on staining with antibodies conjugated with different fluorophores from those used for lineage staining. The resulting population was then analyzed for Thy1 and ST2, and the double-positive cells were considered ILC2s (except skin and small intestine). For skin and small intestine cells, Lin$^-$Thy1.2$^+$CD103$^+$ICOS$^+$ and Lin$^-$Thy1.2$^+$GATA3$^+$RORγt$^-$ populations, respectively, were defined as ILC2s. The bar graph at the bottom shows the average percentages of tdTomato$^+$ ILC2 cells from pooled data of several experiments, and the number of each organ analyzed is as indicated. **(b)** Representative organs of *plck*-Cre; ROSA26-stop-tdTomato; E2A$^{f/f}$; HEB$^{f/f}$ mice were analyzed as described for panel a (n = 4 for each organ). **(c)** Percentage of ILC2s of total CD45$^+$ cells in indicated organs of mice shown (a) and quantified for statistical analysis (b). Student's t test was used to determine statistical significance for each organ. Error bars are SEM. **, P < 0.01; ****, P < 0.0001. Thy, thymus; WAT, white adipose tissue; SiLP, small intestine lamina propria.

Fig. 1. Interestingly, thymic ILC2s from homozygous Id1 transgenic mice (Id1$^{tg/tg}$), which also harbor a large amount of ILC2s in the thymus and elsewhere, did not show TCR rearrangement (Fig. 2, a and b). This is likely because ILC2s in Id1$^{tg/tg}$ mice differentiated from progenitors that have not initiated TCR rearrangement. Although the Id1 and Cre transgenes are both driven by the *lck* proximal promoter, the timing of transgene expression may be different due to their different sites of integration. *plck-Id1* is likely expressed before the DN2 stage, when few DN2 cells were marked by *plck-Cre* (Wang et al., 2009, 2017). As a result, the tdTomato reporter induced by *plck-Cre* labeled a very small fraction (~10%) of thymic ILC2s in heterozygous Id1 transgenic mice, which have a leaky block in T cell development (Wang et al., 2017). We would predict that the thymuses of

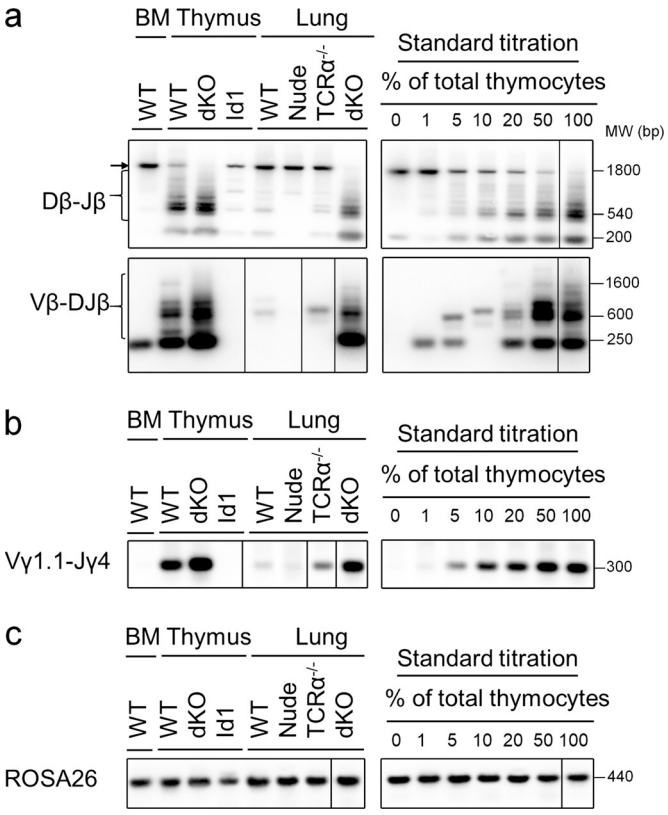

Figure 2. **TCR gene rearrangement in ILC2s.** ILC2s from different organs of C57BL/6J (WT), Id1$^{tg/tg}$ (Id1), *plck*-Cre; E2A$^{f/f}$; HEB$^{f/f}$ (dKO), B6 (SJL)-Foxn1^{nu-2J}; GrsrJ (Nude), and TCRα$^{-/-}$ mice were sorted for DNA preparation. The concentration of each sample was adjusted based on the input number of cells (500 cells/µl). Standard curves were generated by using DNA from mixtures of Mac1^{+} BM cells and total thymocytes. **(a and b)** Rearrangement events of the TCRβ (a) and TCRγ (b) loci were analyzed. Brackets indicate multiple rearranged gene products for TCRβ. Arrow points to the germline product of TCRβ amplified with primers binding to Dβ2 and Jβ2. **(c)** Control for DNA quantity was performed using primers amplifying the ROSA26 gene. Approximate molecular weights of select PCR products are shown on the right. Data shown are representative of at least three experiments.

Id1$^{tg/tg}$ mice have an even lower percentage of tdTomato^{+} ILC2s. In any case, the different status of TCR gene rearrangements between Id1 transgenic and E protein dKO ILC2s suggests that ILC2s can arise from different T cell precursors.

Thymic ILC2s up-regulate ILC2 signature genes while down-regulating T cell–specific genes

Phenotypic studies of Id1 transgenic and E2A/HEB double knockout mice revealed robust ILC2 differentiation in the thymus as a result of loss of E protein function. To examine the changes in the transcriptional profiles as T cell progenitors divert to the innate lymphoid path, we performed RNA sequencing (RNA-seq) analyses of ILC2s isolated from the thymus of Id1$^{tg/tg}$ (Id1) and *plck*-Cre; E2A$^{f/f}$HEB$^{f/f}$ (dKO) mice, respectively. Data were then analyzed in comparison to that of WT DN3 thymocytes (Zhang et al., 2012). As shown in the volcano plots, Id1 and dKO ILC2 each exhibited sets of up- and down-regulated genes relative to DN3 cells, some of which are of particular interests and are highlighted in the plots (Fig. 3 a). The Venn diagram revealed 641 genes that are differentially expressed by both Id1 and dKO ILC2s compared with DN3 cells (Fig. 3 b).

We then focused on this common gene set for further analyses. Unsupervised hierarchical clustering analysis shows two large clusters, designated as clusters 1 and 2 (Fig. 3 c). Cluster 1 contains genes highly expressed in DN3 cells and is represented by a set of genes essential for T cell differentiation (Fig. 3 c). Cluster 2 is enriched in genes up-regulated in both Id1 and dKO ILC2s, many of which are known to be associated with ILC identity and/or function (Fig. 3 c). Additionally, ingenuity pathway analysis (IPA) established connections between these differentially expressed genes and suggested *Zbtb16* and *Id2/3* plus *IL4* as critical nodes (Fig. 3 d). Remarkably, 23 of the ZBTB16 target genes including those essential for ILC2 differentiation (e.g., *Rora* and *Id2*) were included in our differentially expressed gene set (Mao et al., 2016). Taken together, these data suggest that down-regulation of E protein function leads to the switch from T cell to ILC fate.

Committed T cell progenitors can differentiate into functional ILC2s in vitro

To directly test whether committed T cell precursors such as DN3 cells have the potential to differentiate into ILC2s, we used the OP9-DL1 stromal cell coculture system to monitor ILC2 differentiation in vitro (Schmitt and Zuniga-Pflucker, 2002; Constantinides et al., 2014; Yang et al., 2015). Different progenitors (CLP, DN1, and DN3) were sorted from WT mice with high purity (Fig. S2 b), plated onto OP9-DL1 stromal cells, and cocultured in medium containing 30 ng/ml each of IL-2, IL-7, and stem cell factor as described by Yang et al. (2015) (Fig. 4 a). Cultured cells were then analyzed at different time points by staining for surface marker expression after gating out any TCRβ^{+} or TCRγδ^{+} cells. Fig. 4 a illustrates the analysis of the culture on day 10. As ILC2s differentiate, they express ICOS and CD25, but the level of α4β7 is transiently increased and then decreased. Ultimately, ICOS^{+}NK1.1^{-}CD25^{+}α4β7^{-} cells were considered ILC2s (Constantinides et al., 2014). The time course of ILC2 differentiation shown in Fig. 4 b indicated that CLP, DN1, and DN3 all differentiated robustly. On day 7, DN1 and DN3 differentiated at similar efficiencies, whereas CLP lagged behind. At later time points, DN3 cultures plateaued much earlier than DN1 and CLP cultures (Fig. 4 b), probably due to a lower capacity of DN3 cells to expand in this culture condition. The different kinetics could also be used to argue against the notion that ILC2s in the DN3 culture were derived from rare contaminating cells such as DN1 or DN2. Considering the relative abundance of DN3 over DN1 cells, DN3 could contribute to significant proportions of ILC2s generated in the thymus even with a lower capacity on a per-cell basis.

To further exclude the possibility that DN3 cells used to initiate the culture are contaminated with ILC2s or earlier T cell precursors in the thymus, we cultured sorted DN1 or DN3 cells in the medium containing IL-7 and IL-33 with or without IL-2, in comparison to the condition in Fig. 4, a and b. Both DN1 and DN3

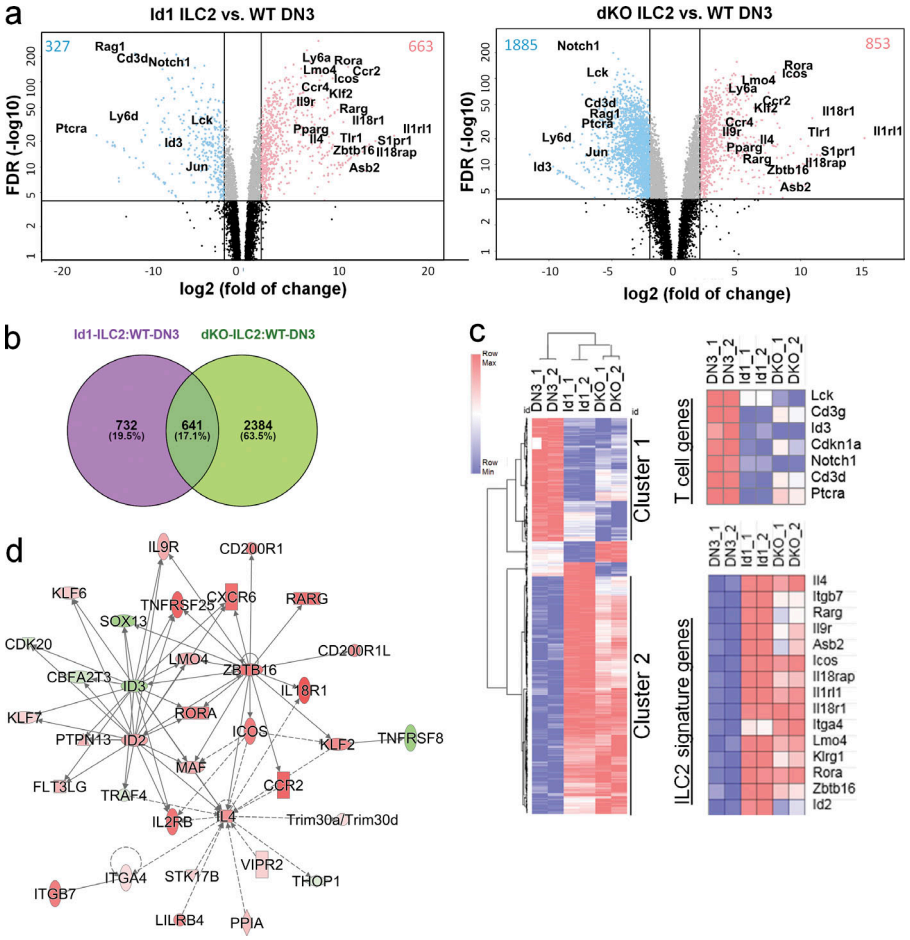

Figure 3. **Thymus ILC2s up-regulate ILC2 signature genes while down-regulating T cell–specific genes.** RNA-seq was performed in duplicates on ILC2s isolated from *plck*-Cre; E2A$^{f/f}$; HEB$^{f/f}$ (dKO ILC2) or Id1$^{tg/tg}$ (Id1 ILC2) mice and compared with data from CD4$^-$CD8$^-$CD44$^-$CD25$^+$ DN3 cells (WT DN3). **(a)** Volcano plots depict differentially expressed genes comparing ILC2 and DN3 cells. Blue and red dots represent genes down- and up-regulated in ILC2 by more than fourfold with FDR < 0.0001, respectively. Genes of interest are labeled. **(b)** Venn diagrams were generated using differentially expressed (DE) genes (more than fourfold and FDR < 0.0001) in the indicated comparison using the Venny 2.1 program. Common DE genes are shown in the overlapping area. **(c)** The heatmap on the left shows the common DE genes (base mean >100) analyzed using unsupervised hierarchical clustering of normalized counts with the Morpheus program. Selected T cell and ILC signature genes are shown on the right. **(d)** IPA shows the top network of the common DE genes. Red and green indicate up- and down-regulated genes, respectively.

cells produced large numbers of ILC2s in medium containing IL-2 and IL-7 plus IL-33 or SCF when measured on either day 10 or 13 (Fig. 4 c). In the absence of IL-2, DN1 cells could generate ILC2s, but DN3 cells failed to do so. The DN3 yield of ILC2 under this condition was less than one cell per input after 13 d, whereas inclusion of IL-2 in the medium allowed ILC2 production at least 600 times more efficiently (Fig. 4 c). These findings are consistent with a previous report which concluded that DN3 cells could not differentiate into ILC2s when supplied with IL-7 and IL-33 only (Wong et al., 2012). Apparently, IL-2 is necessary for ILC2 differentiation from DN3 cells in vitro. This result also ruled out the possibility that ILC2s detected in our original DN3 cultures were due to the expansion of contaminating thymic ILC2s or DN1 cells in the DN3 preparations, which would have expanded in the presence of IL-7 and IL-33.

To functionally verify the identity of these phenotypic ILC2s, we switched the cultured cells to a stroma-free condition in a medium supplemented with ILC2 activating cytokines (IL-25 and IL-33 for 3 d). Both DN1- and DN3-derived ILC2s were capable of producing ILC2 signature cytokines, IL-5 and IL-13, as efficiently as those generated from CLPs, with or without further stimulation with PMA and ionomycin (Fig. 4, d and e). Thus, our results indicated that both multipotent progenitors and committed T cell precursors in the thymus can differentiate into functional ILC2s in vitro.

Loss of E proteins potentiates ILC2 differentiation in vitro and in vivo

As loss of E proteins led to ILC2 expansion in vivo (Fig. 1), we tested its impact on ILC2 differentiation in vitro. We initially isolated DN3 cells from control and *plck*-Cre; E2A$^{f/f}$; HEB$^{f/f}$ mice and placed them in the coculture system described above. After 7 d, E protein–deficient DN3 cells generated many more ILC2s than those from control mice, demonstrating the suppressive effects of E proteins on ILC2 differentiation at the DN3 stage (Fig. S3). However, this experiment could not rule out the possibility that the DN3 cells sorted from the dKO mice were already skewed toward the ILC2 cell fate.

We next employed an inducible system to ablate E proteins by generating ROSA26-CreERT2; ROSA26-stop-tdTomato; E2A$^{f/f}$/HEB$^{f/f}$ mice along with ROSA26-CreERT2; ROSA26-stop-tdTomato mice as controls. The impact of E proteins on ILC2 differentiation from CLP, DN1, and DN3 cells was then evaluated by deleting the two E protein genes with 4-hydroxyltamoxifen (4-OHT) after the initiation of the coculture on OP9-DL1 stromal cells with appropriate cytokines (Fig. 5 a). When 4-OHT was added on day 4 and left in the culture for three more days, it induced efficient deletion as indicated by the expression of tdTomato in 70–90% of the cells (Fig. 5 b). CLPs differentiated more slowly, and the cultures were analyzed on day 14. Loss of E proteins led to a 20-fold increase in the number of ILC2s produced (Fig. 5 c). In contrast, DN1- and

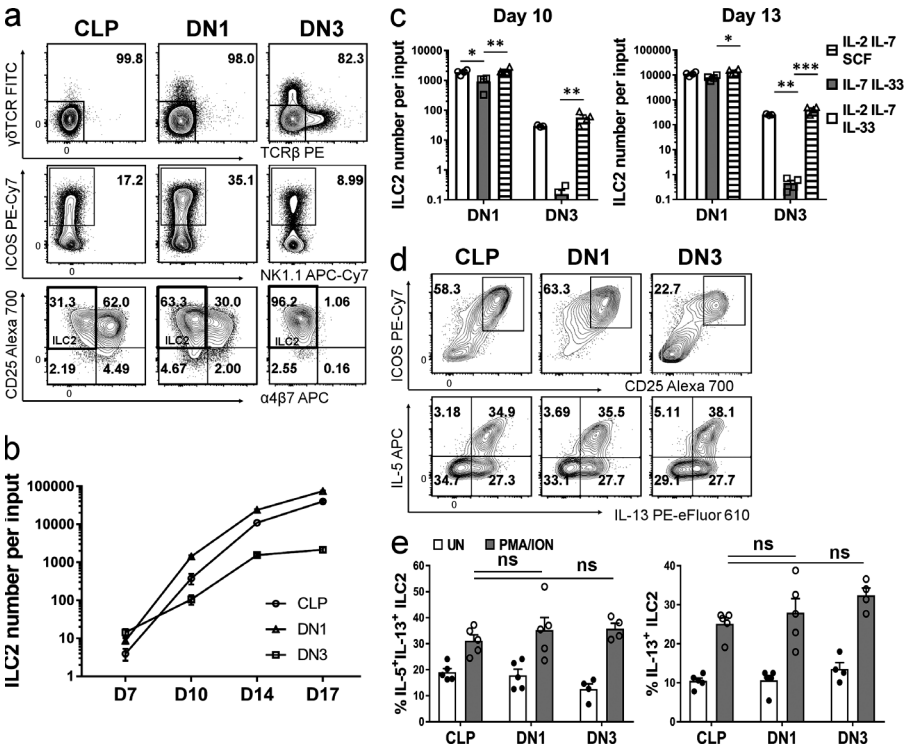

Figure 4. **Committed T cell precursors are able to differentiate into functional ILC2s in vitro. (a)** Progenitors from the BM (CLP) and thymus (DN1 and DN3) were isolated from WT mice and cultured on OP9-DL1 stromal cells in the presence of IL-2, IL-7, and SCF for 10 d. Representative gating strategies for identifying ILC2s generated from indicated progenitors are shown for live CD45$^+$ cells. ILC2s were identified as TCRβ$^-$γδTCR$^-$ICOS$^+$NK1.1$^-$CD25$^+$α4β7$^-$, as labeled in the final gate. **(b)** Time course of ILC2 differentiation from indicated progenitors (n = 4). Data shown are representatives of at least six independent experiments. Two-way ANOVA shows $P < 0.0001$. Error bars are SEM. **(c)** WT DN1 and DN3 cells were set up on OP9-DL1 stromal cells as in panel a with media containing indicated cytokines. The concentration of all cytokines was 30 ng/ml, except that IL-33 was used at 10 ng/ml. ILC2 production at indicated time points was measured as described in panel a. Bar graphs show average percentage of three or four replicates and are representatives of three independent repeats. One-way ANOVA was used for statistical analyses. Error bars are SEM. *, $P < 0.05$; **, $P < 0.01$; ***, $P < 0.001$. **(d)** Cytokine production was measured after incubating cells from the 14-d coculture as in panel a for three more days in stromal-free medium supplemented with IL-2, IL-7, IL-33, and IL-25 followed by PMA plus ionomycin stimulation for 2 h. IL-5 and IL-13 production in TCRβ$^-$γδTCR$^-$ICOS$^+$CD25$^+$ ILC2 cells was determined. **(e)** Quantification of percentages of IL-13$^+$ and IL-5$^+$IL-13$^+$ ILC2 as shown in panel d. Cytokine production without treatment with PMA and ionomycin was also measured as included in the graph. Bar graphs show average percentage of replicates (n = 4) of one of three independent experiments. One-way ANOVA was used to determine statistical significance between DN1 or DN3 and CLP cultures after PMA plus ionomycin stimulation. Error bars are SEM. One-way ANOVA was used for statistical analyses. ns, not significant.

DN3-derived cells could be evaluated on day 11, and E protein deficiency resulted in 42- and 30-fold enhancement in ILC2 differentiation, respectively (Fig. 5, d and e). These results thus suggest that E proteins can suppress the ILC2 cell fate at multiple stages of T lymphopoiesis, including a committed T cell precursor stage, DN3. In addition, these E protein–deficient ILC2s were capable of producing IL-5 and IL-13 efficiently in response to stimulation with IL-25 and IL-33 (data not shown).

Using similar inducible mouse models, we next evaluated the effects of inducible E protein ablation in vivo (Fig. 6). To delete E protein genes, tamoxifen was administered daily to 3-wk-old E2A$^{f/f}$HEB$^{f/f}$ mice with or without the ROSA26-CreERT2 transgene for 9 d and analyzed 6 d after the last dose of tamoxifen (Fig. 6 a). This regimen was found to be highly efficient in Cre-mediated deletion when tested by using ROSA26-CreERT2; ROSA26-stop-tdTomato; E2A$^{f/f}$/HEB$^{f/f}$ and ROSA26-CreERT2; ROSA26-stop-tdTomato mice (data not shown). In the BM, the number of ILC progenitors increased more than twofold in E protein–deficient mice compared with controls (Fig. 6 a). Furthermore, the number of newly made ILC2s, called ILC2Ps (Hoyler et al., 2012; Yu et al., 2014), was boosted fivefold by E protein ablation (Fig. 6 a). These changes were accompanied by a reduction in B lymphopoiesis but not in myeloid differentiation (Fig. 6 a). In the thymus, ILC2 levels increased ∼10-fold due to E protein deficiency (Fig. 6 a). Like the situation in the BM, this was concomitant with diminished T cell production, as the numbers of T cells at all developmental stages were dramatically reduced (Fig. 6 a and data not shown). Finally, we detected a 10-fold increase in ILC2 counts in peripheral organs such as the lung. This is likely due to increased output from the BM and thymus, although we have not yet ruled out enhanced local expansion.

With regard to other immune cell types, we examined their production in the BM and thymus of these inducible mice (Fig. 6 b). BM ILC1 and ILC3 were found to be unaltered upon E protein deletion. However, the numbers of dendritic lineage cells including pre-conventional DC (cDC) and plasmacytoid dendritic cells (pDCs) decreased, consistent with the known function of E proteins in the differentiation of these cells (Cisse et al., 2008; Kee, 2009; Sichien et al., 2016). BM NK cells were also diminished, probably as a result of increased divergence of CLPs toward the innate lymphoid lineages, specifically ILC2s. Thymic NK levels were similar with or without E protein deletion. We also determined the ability of DN thymocytes in these inducible mice to generate cytokines known to be produced by NK and ILC lineage cells (Fig. 6 c). With the exception of IL-5 and IL-13, we did not see any marked increase in IL-17, IL-22, IFNγ, or IL-4 expression. Collectively, these data suggest that the levels of E proteins are specifically crucial for restraining ILC2 differentiation.

Transcriptional profiling at early stages of ILC2 differentiation

To understand the changes in gene expression at the onset of ILC2 differentiation and the impact of E protein deficiency, we

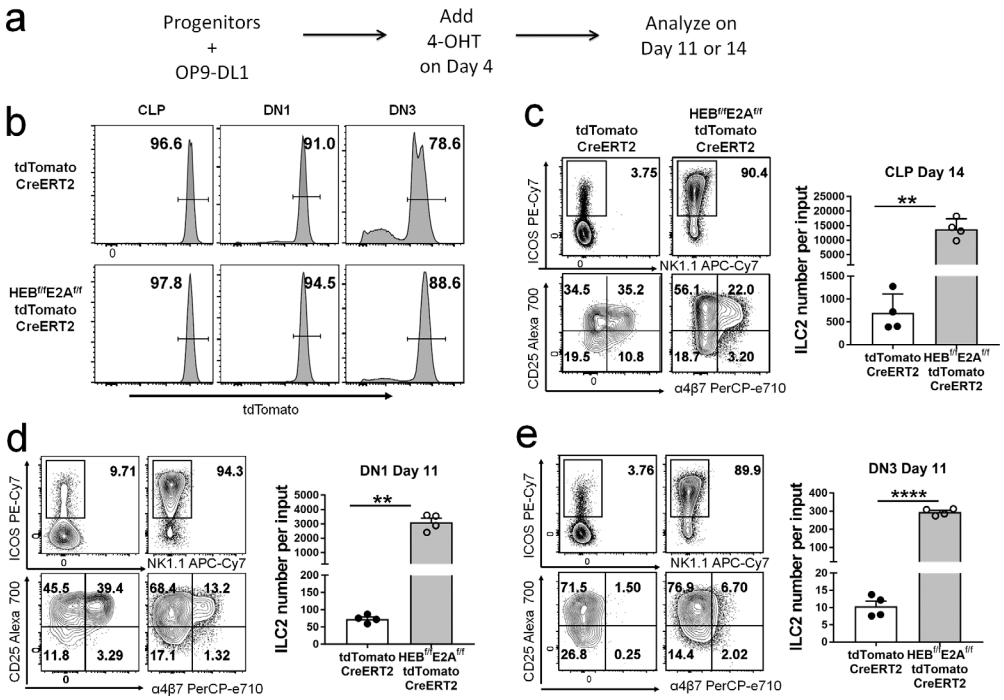

Figure 5. **ILC2 differentiation is enhanced by ablation of E proteins in vitro. (a)** The experimental scheme. CLP, DN1, and DN3 cells were sorted from indicated strains of mice and placed onto OP9-DL1 stromal cells for coculture as described in Fig. 4 a. On day 4, 4-OHT was added to induce CreERT2 function. **(b)** Efficiency of induction by tamoxifen in culture. Expression of tdTomato in $CD45^+$ cells were measured 3 d after addition of 4-OHT and shown in histograms. **(c–e)** Live $CD45^+tdTomato^+TCR\beta^-\gamma\delta TCR^-$ cells from CLP (c), DN1 (d), and DN3 (e) cocultures were analyzed, and the gating strategies of ILC2s are shown. Numbers of $tdTomato^+$ ILC2s per input of indicated progenitors at indicated time points are shown on the right ($n = 4$). Data shown are representative of two experiments. Student's *t* test was used to determine statistical significance. Error bars are SEM. **, $P < 0.01$; ****, $P < 0.0001$.

took advantage of the in vitro differentiation system and performed RNA-seq analyses in a time course. DN1 and DN3 thymocytes were isolated from ROSA26-CreERT2; ROSA26-stop-tdTomato and ROSA26-CreERT2; ROSA26-stop-tdTomato; $E2A^{f/f}/HEB^{f/f}$ mice. These cells were placed on OP9-DL1 stromal cells in the presence of IL-2, IL-7, and SCF as described for Fig. 5. On day 4, 4-OHT was added after an aliquot was collected for RNA isolation. On days 5 and 7, aliquots of cells were harvested, and $tdTomato^+$ cells, which are presumed to have undergone Cre-mediated deletion, were sorted for RNA isolation (Fig. 7 a). At these time points, $tdTomato^+$ cells were also scored for ILC2 differentiation (Fig. S4).

To evaluate the data, we first took a candidate approach and examined the expression profiles of genes known to be related to ILC2 differentiation (Fig. 7 b). Although few phenotypic ILC2s were detected on day 5, expression of a number of genes began to increase within 24 h after the initiation of E protein gene deletion, but not in the control cells. On day 7, the levels of these genes in dKO cells continued to rise while the controls barely began to up-regulate them. In general, DN1 and DN3 displayed similar patterns of gene expression in these analyses, with minor variations mainly attributed to the different basal levels in DN1 and DN3 cells on day 4. Strikingly, several transcription factor genes, including *Zbtb16*, *Gata3*, *Rora*, *Tox*, and *Lmo4*, were induced shortly following E protein ablation on day 5, but they only became noticeable on day 7 in control cells. As a result, an array of their downstream targets such as *Icos*, *IL4*, *Il9r Il18r*, and *Il18rap* and *Id2* were also up-regulated. *Itga4* and *Itgb7* are known be regulated by IL-4 signaling and were also dramatically increased in dKO cells. Interestingly, *IL2r* and *IL7r* were highly expressed in both dKO and control DN1-derived cells. Although cytokines for these receptors were supplied in the culture, IL-2 and IL-7 signals alone are not sufficient to drive robust ILC2 differentiation. For DN3-derived cells, *Il2ra* expression was preferentially up-regulated in dKO cells. Likewise, *Tcf7* expression did not appear to be a rate-limiting factor for ILC2 differentiation comparing dKO and control cells.

To identify sets of genes that behaved similarly over the time course, we used the Hierarchical Ordered Partitioning and Collapsing Hybrid (HOPACH) algorithm (see Materials and methods), which grouped 3,938 of the 22,000 genes examined into six clusters for both DN1- and DN3-initiated cultures. While changes in gene expression for groups 1, 4, and 6 were rather modest, genes in groups 3 and 5 were continuously up-regulated, and group 2 genes were down-regulated during the course of differentiation. Interestingly, the genes shown in Fig. 7 b all belonged to group 3 except *Id2*, *Rarg*, *Tcf7*, and *Il7r*, suggesting that this group of genes are closely related to ILC2 differentiation. Indeed, IPA showed that group 3 genes are associated with T helper cell differentiation and activation, glycolysis, and ICOS-ICOSL signaling (Fig. S5 a), and it also revealed the regulatory networks centered on ZBTB16, GATA3, STAT1, and STAT3 transcription factors, as well as on IL-4 and IL-2 signaling pathways (Fig. S5 b).

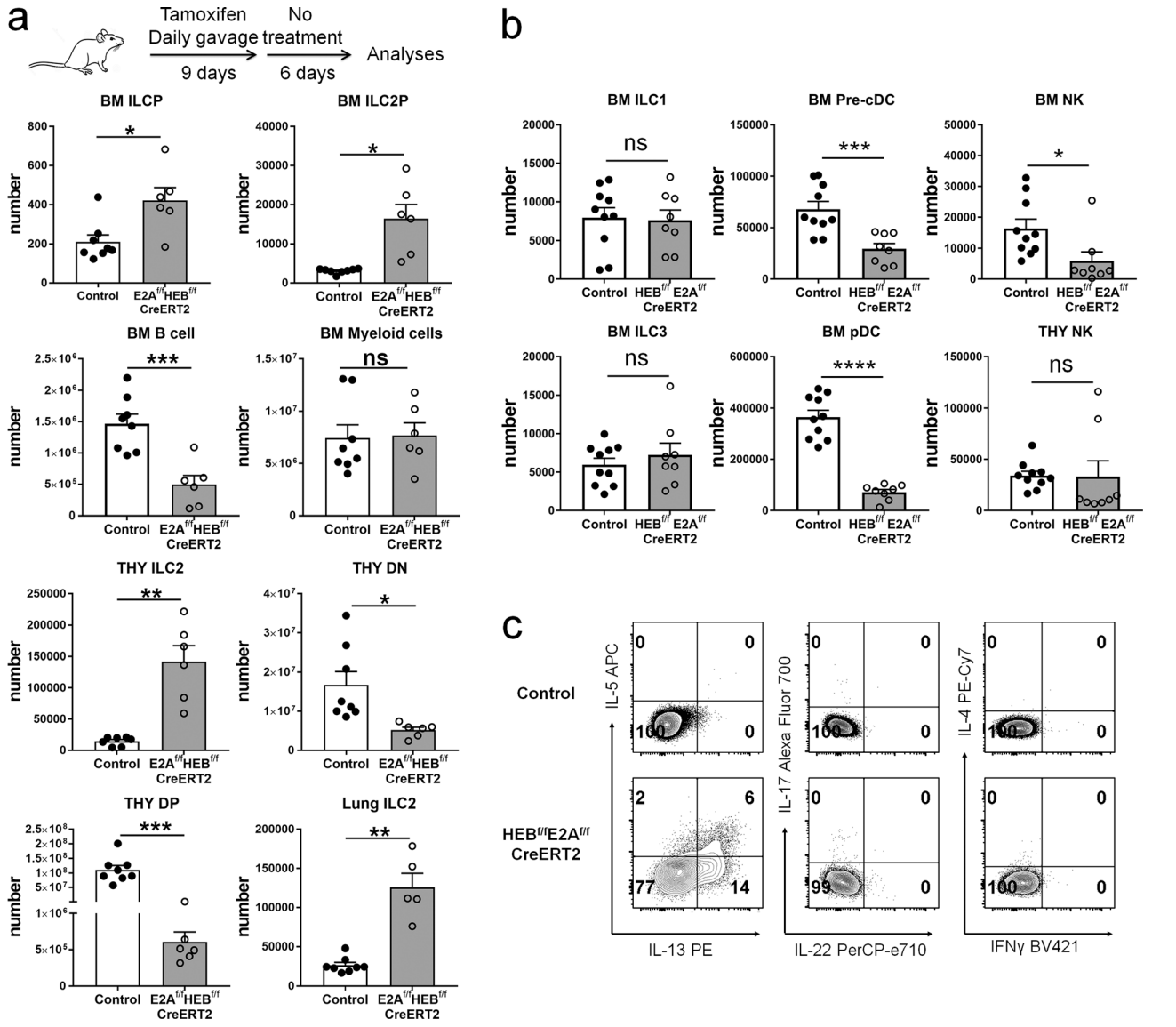

Figure 6. **Inducible ablation of E proteins promotes ILC2 differentiation in vivo. (a)** ROSA26-CreERT2; $E2A^{f/f}$; $HEB^{f/f}$ and control ($E2A^{f/f}$; $HEB^{f/f}$ or ROSA26-CreERT2) mice were treated to induce the deletion of E proteins as diagrammed on the top. The definitions of the BM populations are ILCP ($Lin^-Thy1.2^+IL\text{-}7^+ST2^-Sca\text{-}1^-cKit^+\alpha4\beta7^+PD\text{-}1^+$), ILC2P ($Lin^-Thy1.2^+IL\text{-}7^+ST2^+Sca\text{-}1^+CD25^+\alpha4\beta7^+$), B cells ($B220^+CD19^+$), and myeloid cells ($Mac\text{-}1^+$). ILC2s in the thymus and lung are $Lin^-Thy1.2^+ST2^+$. Total cell numbers of each indicated subset were quantified. Data shown are pooled from three experiments (n = 5–8). **(b)** Lineage cocktails for BM ILC1, BM ILC3, and BM NK include antibodies against FcεRI, B220, CD19, Mac-1, Gr-1, Ter-119, CD3ε, CD5, and CD8α. BM ILC1 were defined as $Lin^-Thy1.2^+IL\text{-}7R^+CD62L^-CD27^+ST2^-$; BM ILC3 as Lin^- $Thy1.2^+IL\text{-}7R^+CD62L^-CD27^-ST2^-$; and BM NK as $Lin^-Thy1.2^+IL\text{-}7R^-CD62L^+NK1.1^+DX5^+$. Lineage markers for BM pre-cDC and BM pDCs are CD3, CD8α, CD5, TCRβ, γδTCR, NK1.1, Ter119, and Ly6G. BM pre-cDCs were gated as $Lin^-B220^-MHCII^-CD11c^+Flt3^+Sirp\alpha^-$ and BM pDCs as $Lin^-B220^+CD19^-SiglecH^+$. Thy NKs were considered as Lin (CD3, CD8α, CD4, TCRβ, γδTCR)$^-CD122^+NK1.1^+DX5^+$. Data shown are pooled from three independent experiments (n = 8–10). Student's t test was used to determine statistical significance. Error bars are SEM. *, $P < 0.05$; **, $P < 0.01$; ***, $P < 0.001$; ****, $P < 0.0001$; ns, not significant. **(c)** Thymocytes from mice used in panel a were cultured in the presence of PMA and ionomycin plus monensin for 4 h before intracellular staining and analyzed with indicated antibodies. Data shown are representatives from two independent experiments.

Group 5 contains genes involved in DNA repair and cell cycle regulation, but the statistical significance (P values) of these changes were several orders of magnitude lower than those in group 3 (Fig. S5 a). Group 2 encompasses large sets of down-regulated genes related to cell migration and cell adhesion. However, the interpretation of this group of genes may be complicated by a potential contamination of stromal cells in the day 4 samples.

Distinct functionalities of thymus-derived ILC2s

Principal component analyses revealed that ILC2s from different progenitors or in different tissues exhibit diverse transcriptomes to a varying degree (Fig. 8 a). Although lung ILC2s from WT, Id1, and dKO mice are similar relative to other ILC2 populations, they exhibit differences in their transcriptional profiles among themselves, which suggest that they may possess distinct functions. Histological examination of lung tissues of

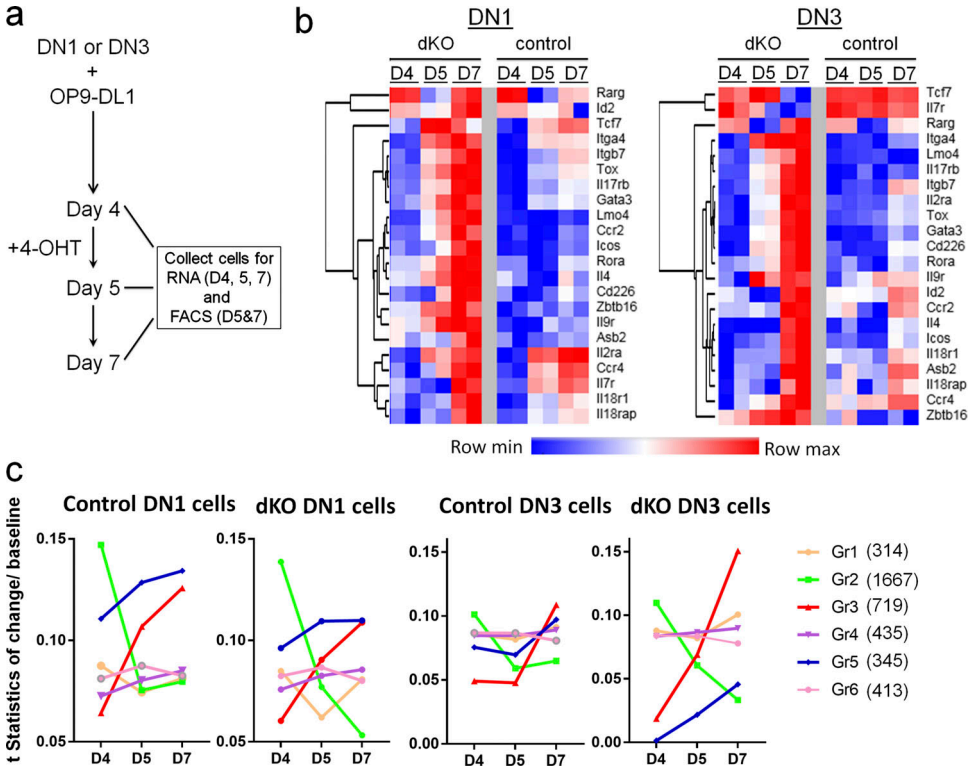

Figure 7. **Transcriptional profiling at the early stages of ILC2 differentiation. (a)** Experimental scheme. DN1 and DN3 thymocytes from ROSA26-CreERT2; ROSA26-stop-tdTomato; E2A$^{f/f}$; HEB$^{f/f}$ (dKO) and ROSA26-CreERT2; ROSA26-stop-tdTomato (control) mice were cocultured as in Fig. 5 a. Biological duplicates were collected on days 4 (D4), 5 (D5), and 7 (D7) for RNA isolation for RNA-seq. D5 and D7 cells were sorted for tdTomato expression. **(b)** Normalized read counts of candidate ILC signature genes in DN1- or DN3-initiated cultures were plotted in heatmaps with unsupervised hierarchical clustering using the Morpheus program. **(c)** Gene expression variation profiles over the time course. Six groups of similar expression variation profiles were identified among 3,938 genes, using the HOPACH algorithm. Trends of gene expression changes are depicted in color-coded lines, and the numbers next to the legend of each line show the number of genes in each group.

2-mo-old mice revealed widespread spontaneous infiltration of immune cells near vasculatures in Id1 and dKO mice, resembling the lung pathology caused by IL-33 administration (Fig. 8 b; Zhiguang et al., 2010; Li et al., 2014). Whether this is simply due to the overabundance of ILC2 in the lung of these mutant mice or reflects any functional differences remains to be further investigated.

We have previously demonstrated heightened type 2 immunity during parasite infection and allergen challenge in Id1 mice, but it was not clear if this was due to a cell-intrinsic effect or because of the increased ILC2 counts (Wang et al., 2017). We therefore compared the responses of lung ILC2s isolated from WT, Id1, and dKO mice to ILC2 activators in vitro. Equal numbers of cells were initially plated in medium containing IL-2 and IL-7 with or without IL-25 or IL-33 and cultured for 3 d. Interestingly, Id1 and dKO ILC2s proliferated much faster when IL-25 or IL-33 was added (Fig. 9 a). Staining for Ki67 also confirmed the higher proliferative potential of these cells under these conditions (Fig. 9, b and c). Moreover, there was a striking difference in the percentage of Ki67$^+$ cells in cells cultured with IL-2 and IL-7. Only ∼10% of WT ILC2s were Ki67$^+$, but Id1 and dKO cells had 40% (Fig. 9, b and c). Although Ki67 expression in ex vivo lung ILC2s of all three genotypes are very low (Fig. 9 d), WT cells remains in the resting state, while a large fraction of Id1 and dKO cells are ready to proliferate before stimulation with IL-25 or IL-33, suggesting that Id1 and dKO ILC2s are more poised for expansion if given appropriate stimuli.

With regard to the abilities to produce type 2 cytokines when exposed to ILC2 activators, we performed intracellular staining to measure the responses on an individual cell basis and ELISA to gauge the collective outcomes. In the presence of IL-2 and IL-7 alone, very few cells expressed IL-5 or IL-13 (Fig. 10 a). Addition of IL-25 stimulated cytokine production more robustly in Id1 and dKO cells, whereas IL-33 was more effective on WT ILC2s (Fig. 10 a). Analyses of mean fluorescence intensity of IL-5$^+$ or IL-13$^+$ cells revealed that Id1 and dKO ILC2s express slightly higher levels of IL-5 and IL-13 in the presence of IL-25 but WT ILC2s produced significantly higher levels of cytokines when cultured in IL-33 (Fig. 10 b). This result is consistent with the ELISA data which shows the accumulation of IL-5 and IL-13 in the course of 3 d (Fig. 10 c). Relative to WT cultures, Id1 and dKO cultures had higher levels when stimulated with IL-25 but lower levels in the presence of IL-33. We note that the cell numbers at the end of the culture with the three genotypes were different, which would impact cytokine yields. However, it is difficult to simply calculate cytokine production on a per-cell basis due to the unknown kinetics of cytokine secretion and stability of the cytokines. Nevertheless, the trends are that Id1 and dKO ILC2s

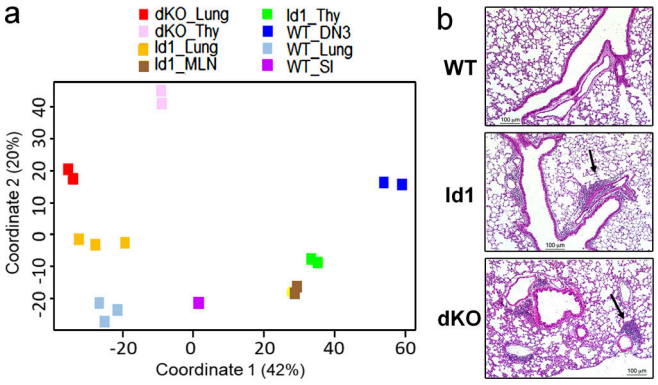

Figure 8. **Distinct ILC2 transcriptomes and lung histology of WT, Id1, and dKO mice. (a)** Principal component analysis of ILC2 transcriptomes from different organs of C57BL/6J (WT), $Id1^{tg/tg}$ (Id1), and *plck*-Cre; $E2A^{f/f}$; $HEB^{f/f}$ (dKO) mice using 2D multidimensional scaling representation. Expression profiles of 5,456 genes, deferentially expressed between at least two of the sample types under study, were used in computing distances. Percentages show proportion of total distance among all samples, captured by each axis. Thy, thymus; SI, small intestine. **(b)** Hematoxylin and eosin staining of lung tissues from 2-mo-old mice of the indicated genotypes. Arrows indicate immune cell infiltration. Scale bars represent 100 µm. Representative graphs from three mice of each genotype are shown.

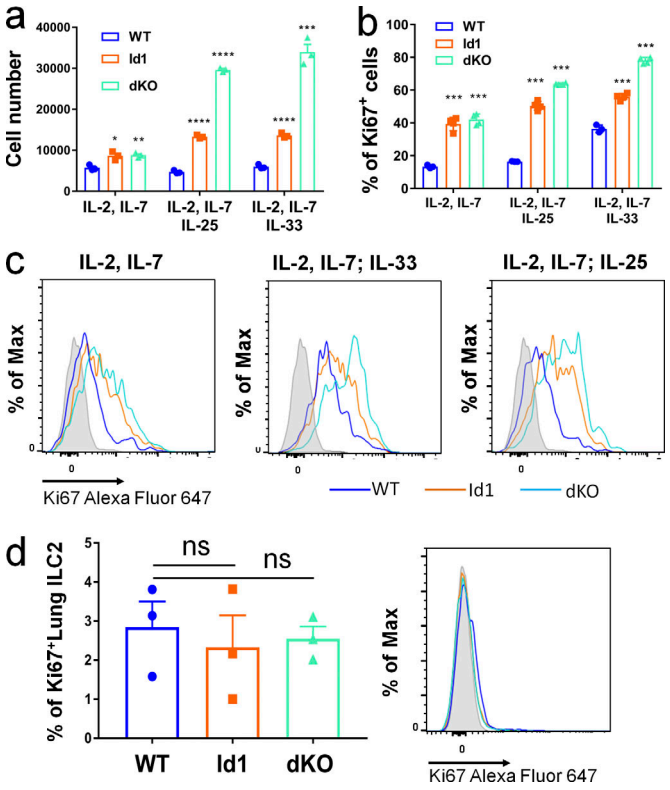

Figure 9. **Increased proliferative potential of lung ILC2s of Id1 and dKO mice.** Sorted lung ILC2s (4,000 cells) from mice of indicated genotypes were cultured for 3 d in the presence of 10 ng/ml each of IL-2 and IL-7 ± 10 ng/ml IL-25 or 1 ng/ml IL-33. 400,000 $CD45.1^+$ thymocytes were added as carriers at the time of the flow cytometry analyses, and counting beads were used to determine the $CD45.2^+$ cell numbers. Based on the recovery of $CD45.1^+$ cells, it was estimated that the intracellular staining procedures caused a 50% loss of the cells. **(a and b)** Cell counts (a) and percentages (b) of $CD45.2^+Ki67^+$ cells are shown (n = 3). Data shown are representatives from two to three independent experiments. Student's t tests were used to determine the statistical significance between WT and mutant cells. Error bars are SEM. *, $P < 0.05$; **, $P < 0.01$; ***, $P < 0.001$; ****, $P < 0.0001$. **(c)** Representative intracellular staining profiles for Ki67 expression in lung ILC2s cultured in the indicated conditions. Data shown are representative graphs from two independent experiments. The solid peak shows the negative control for anti-Ki67 staining. Blue line, WT; orange line, Id1; cyan line, dKO. **(d)** Ki67 staining of freshly isolated lung ILC2s. Student's t tests were used to determine the statistical significance. ns, not significant.

are slightly more responsive to IL-25 than WT cells, whereas WT cells are more sensitive to IL-33.

We also evaluated the responses of these ILC2s to two well-known neuropeptides, neuromedin U (NMU) and vascular intestinal peptide (VIP), in the presence of IL-2, IL-7, and IL-25 (Nussbaum et al., 2013; Klose et al., 2017; Wallrapp et al., 2017). NMU and VIP did not stimulate cytokine production without IL-25 (data not shown). Under the condition we used, we saw slight additional boost by NMU in WT and dKO cells, but VIP appeared to have significantly synergistic effects on all three genotypes (Fig. 10 d). Collectively, these in vitro analyses revealed some functional differences between WT and Id1 or dKO ILC2s, which could shed light on the potential functional specialization of thymus-derived ILC2s.

Discussion

The capacity of the thymus to generate ILC2s has been demonstrated here and elsewhere (Miyazaki et al., 2017; Wang et al., 2017; Bornstein et al., 2018; Jones et al., 2018; Kernfeld et al., 2018). The thymic environment is known to provide ample Notch and IL-7 signals needed for ILC2 differentiation, and the recent identification of IL-25–producing thymic tuft cells also provokes further interest (Gentek et al., 2013; Bornstein et al., 2018). While it is not surprising that DN1 thymocytes, which include early thymic progenitors with multipotent potential (Bell and Bhandoola, 2008), can give rise to ILC2, the ability of DN3 thymocytes to do so is unexpected. A previous study showed that DN3s were unable to generate ILC2s when cultured in IL-7 and IL-33 (Wong et al., 2012). We now show that IL-2 is instrumental for the differentiation, survival, and/or expansion of DN3-derived ILC2s in vitro. The existence of DN3-derived ILC2s in WT mice was illustrated by tdTomato labeling with the *plck*-Cre transgene, which is expressed mainly after the DN3 stage (Shi and Petrie, 2012; Wang et al., 2017), and by the detection of TCRβ and TCRγ gene rearrangement events in thymic and lung ILC2s (Figs. 1 and 2). The fact that rearrangement events were detected in lung ILC2s of mice without the majority of T cells ($TCR\alpha^{-/-}$) but not in mice without the thymus further strengthens our conclusion. DN3 cells have not previously been shown to give rise to any non–T lineage cells. Our observation may suggest that ILCs are closer to T cells than any other cell types. A small fraction of NK cells was previously shown to be made in the thymus and contains TCRγ but not TCRβ gene rearrangement (Veinotte et al., 2006). However, DN1 thymocytes were shown to give rise to these cells (Veinotte et al., 2006; Vargas et al., 2011).

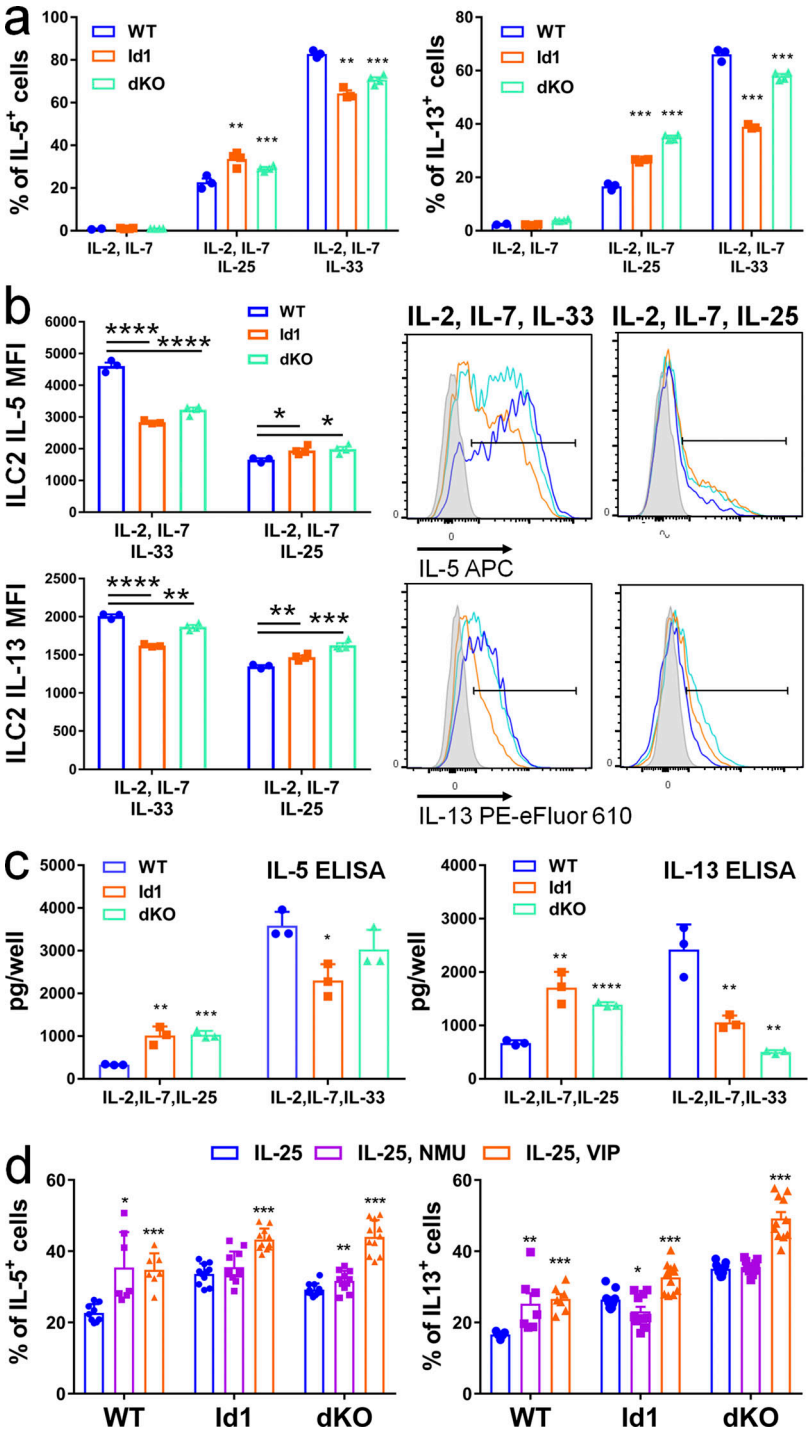

Figure 10. **Different responses of Id1 and dKO ILC2s to activators. (a)** Percentages of IL-5$^+$ or IL-13$^+$ cells were determined by intracellular staining after 4-h monensin block of cells cultured as described for Fig. 9. Data shown are representative results of three independent experiments. Student's *t* test was used to determine statistical significance between Id1 or dKO and WT ILC2. Error bars are SEM. **, P < 0.01; ***, P < 0.001. **(b)** Mean fluorescence intensity of IL-5 and IL-13 in cultured lung ILC2s was determined in the positive gates as shown. Solid peak shows levels of IL-5 or IL-13 staining in cells cultured in IL-2 and IL-7 only. Blue line, WT; orange line, Id1; cyan line, dKO. Data shown are representative results of three independent experiments. Student's *t* test was used to determine statistical significance between Id1 or dKO and WT ILC2. Error bars are SEM. *, P < 0.05; **, P < 0.01; ***, P < 0.001; ****, P < 0.0001. **(c)** ELISA analyses of IL-5 and IL-13 levels before addition of monensin were performed using culture supernatants. The concentrations of IL-5 and IL-13 were calculated based on standard curves. The levels of the cytokines in cells cultured with IL-2 and IL-7 only were below the background. Data shown are representative results of three independent experiments. Student's *t* test was used to determine statistical significance between Id1 or dKO and WT ILC2. Error bars are SEM. *, P < 0.05; **, P < 0.01; ***, P < 0.001; ****, P < 0.0001. **(d)** Intracellular staining for IL-5 and IL-13 in cells cultured in IL-2, IL-7, and IL-25 with or without 1 µg/ml of NMU or 1 µM VIP. Data shown are aggregates of three independent experiments after normalization. Student's *t* test was used to determine statistical significance between Id1 or dKO and WT ILC2. Error bars are SEM. *, P < 0.05; **, P < 0.01; ***, P < 0.001.

Deletion of the E2A and HEB genes using the p*lck*-Cre transgene resulted in a massive expansion of ILC2s with TCRγ and TCRβ rearrangement, suggesting that ILC2 differentiation occurred in committed T cell precursors. In contrast, thymic ILC2s from Id1 transgenic mice did not show much TCR rearrangement (Fig. 2) and were poorly labeled by tdTomato (Wang et al., 2017). This is likely because Id1-driven ILC2 differentiation occurs at a much earlier stage before the initiation of TCR rearrangement, or that Id1 inhibits RAG gene expression and/or reduces the accessibility of the TCR loci. Despite the different developmental stages at which ILC2s were generated in Id1 transgenic and E protein–deficient mice, their ILC2s share a common set of genes known to be related to ILC2 identity and function, thus suggesting that ILC2 differentiation can take place at multiple developmental stages. E proteins are obviously forceful in suppressing the ILC2 fate while driving T cell differentiation. However, T cell precursors, which have lower E protein activity due to elevated amounts of Id protein, increased E protein turnover, or lower levels of E protein expression, can diverge to the ILC2 path. Indeed, up-regulation of Id3

transcription and ubiquitin-mediated degradation of E proteins transiently occur following preTCR signaling (Bain et al., 2001; Nie et al., 2003), thus creating an opportunity for ILC2 digression.

Expression of the tdTomato reporter allowed us to trace the destinations of the DN3-derived ILC2s. The frequency of tdTomato$^+$ ILC2s in the blood is readily detectable, which suggests that thymic ILC2 can egress and circulate in the blood (Fig. 1 a). The tdTomato$^+$ ILC2s seen in the blood depended on the thymus, as nude mice transplanted with BM progenitors of *plck*-Cre; ROSA26-Stop-tdtomato mice had few such cells (Fig. 1 b). Since ILC2s in both Id1 transgenic and E protein–deficient mice express high levels of S1pr1 (Fig. 3 a), which encodes the receptor known to facilitate the egress of mature T cells (Allende et al., 2004; Matloubian et al., 2004), they have the means of exiting the thymus. Although the half-life of these cells and their tissue preference are not entirely clear, we did detect tdTomato expression in small fractions of ILC2s in the lung and skin, suggesting these cells and possibly other unlabeled thymic ILC2s can home to the periphery and participate in immune functions. While this tdTomato reporter provided us with an easy tool for identifying thymus-derived ILC2s, there are some limitations. tdTomato expression negatively impacts cell proliferation or survival. Although thymus specific, the timing of *plck-Cre* expression during T cell development was also not uniform, thus causing some degree of variation in the frequencies of tdTomato$^+$ ILC2s among individual mice. An alternative marker for thymus-derived ILC2s would greatly aid further investigation.

Comparison of transcriptional profiles between Id1 transgenic or E protein–deficient ILC2 and WT DN3 thymocytes led to the identification of a common set of differentially expressed genes, which includes genes specific for T cell differentiation and genes related to ILC fates. Data from ILC2 cultures also suggest that DN1 and DN3 cells share a common regulatory network during ILC2 differentiation. Interestingly, this gene set includes several genes encoding key transcription factors for ILC differentiation, *ZBTB16*, *Rora*, and *Lmo4* (Fig. 3 c). *Gata3*, though important for ILC2 differentiation (Hoyler et al., 2012; Yagi et al., 2014), is not among them because it is widely expressed in T cells. Furthermore, analyses of gene expression during the initiation of ILC2 differentiation in vitro also revealed the up-regulation of a similar set of transcription factors plus GATA3 and Tox (Fig. 7, b and c). It is amazing that ablating E2A and HEB for <24 h led to concerted up-regulation of all of these transcription factors along with their downstream targets. As a result, E protein–deficient cells have a tremendous advantage in ILC2 differentiation in culture. How E proteins impact the expression of all of these transcription factors is not understood, and it is unreasonable to expect E proteins to repress the target genes individually. However, E proteins have been shown to bind upstream of the promoter of *Zbtb16* and activate transcription in NKT cells (D'Cruz et al., 2014). Whether they play a repressive role in the context of ILC precursors remains to be investigated. ZBTB16 is found in this study to be a major focal point of the transcriptional network and could thus be a prime candidate to be regulated by E proteins. Although loss of ZBTB16 function does not abolish ILC production (Constantinides et al., 2014), gain of its function could promote ILC2 differentiation. In addition, E proteins have previously been shown to repress the transcription of *gata3* (Xu et al., 2013), which could help explain how loss of E proteins leads to up-regulation of GATA3 and ILC2 differentiation in vitro. However, it is equally possible that E proteins up-regulate other transcriptional repressors and non-coding RNAs to suppress the innate lymphoid fate.

Apart from the key transcription factors, cytokine signaling also plays important roles in ILC2 differentiation. Particularly, IL-4 signaling is another node in the regulatory network revealed by analyses of both ex vivo thymic ILC2 and ILC2s generated in vitro. Even though IL-4 secretion is not a major function of ILC2s, its signaling pathway and downstream events might be crucial for ILC2 differentiation, just as they are for Th2 polarization. In contrast, IL-2 and IL-7 are essential for the survival and expansion of ILC2, but they may not dictate the lineage fates of adaptive versus ILCs.

Principal component analysis of bulk RNA-seq data of ILC2s from different tissues of WT, Id1, or dKO mice shows distinct transcriptional profiles. Id1 and dKO ILC2s from the thymus display drastically different patterns, probably reflecting the different cell origins from which they arise (DN1 and DN3, respectively). However, when these cells reach the lung, tissue environment shapes their transcriptomes and makes them less different compared with when they initially develop in the thymus. These observations are consistent with those made using single-cell RNA-seq, where Ricardo-Gonzalez et al. (2018) illustrated different transcriptomes of ILC2s in different tissues and their different dependence on cytokines. Despite the similarity of lung ILC2s of different genotypes, Id1 or dKO ILC2s also exhibit somewhat different transcriptional profiles compared with WT ILC2s, which could lead to functional differences.

To examine cell-intrinsic functions, we compared their responses to IL-25 or IL-33 as well as neuropeptides between ILC2s from WT and Id1 or dKO mice in vitro. Remarkably, Id1 and dKO ILC2s proliferated much more avidly compared with WT ILC2s, probably due to their higher propensity to be at an active state (G1 or G2-M phases) even without IL-25 or IL-33 stimulation. In terms of ILC2 activation by their activators, Id1 or dKO cells are slightly more sensitive to IL-25 but less responsive to IL-33. Likewise, these cells can be further activated by VIP together with IL-25, while NMU had little synergistic effect. Whether these differences found in vitro can be related to in vivo situations and whether Id1 or dKO ILC2s can represent WT thymus-derived ILC2s await further investigation. These tasks will be greatly aided by the availability of specific markers for different subsets of ILC2s, and mutant mice lacking or enriched with thymus-derived ILC2s will be helpful in delineating the different characteristics of the heterogeneous population of ILC2s in peripheral tissues.

Our discovery of the great capacity of the thymus to generate ILC2s from different T cell precursors brings to attention the heterogeneity of ILC2 pools in the periphery and provokes further inquiries into any unrecognized functional differences among different ILC2 subsets derived from the thymus and BM, as well as during embryogenesis. These functional differences,

once understood, could help explain the protective and harmful effects of ILC2s in various pathophysiological situations.

Materials and methods

Mice

C57BL/6J, p*lck*-Cre, Rosa26-STOP-tdTomato, Rosa26-CreERT2, B6.129S2-*Tcra*^{tm1Mom}/J (TCRα$^{-/-}$), and B6(SJL)-Foxn1$^{nu\text{-}2J}$; GrsrJ (nude) mice were purchased from the Jackson Laboratory. p*lck*-Id1 transgenic mice (Kim et al., 1999) and p*lck*-Cre; E2A$^{f/f}$; HEB$^{f/f}$ (Wojciechowski et al., 2007) were as described. All animal experiments were performed according to protocols approved by the Institutional Animal Care and Use Committee policies at the Oklahoma Medical Research Foundation.

Isolation of hematopoietic cells from nonlymphoid tissues

Perfused lungs were cut into small fragments and digested in Hepes buffer (150 mM NaCl, 5 mM KCl, 1 mM $MgCl_2$, 1.8 mM $CaCl_2$, and 10 mM Hepes) containing 25 µg/ml Liberase TH (Sigma) and 10 U/ml DNase I (Sigma) at 37°C for 30 min. Cells were filtered with a 70-µm cell strainer.

White adipose tissue was cut into small pieces and digested in DMEM containing 200 µg/ml collagenase IV and 3% BSA at 37°C for 30 min while shaking. Then, HBSS containing 0.5% BSA was used to stop the reaction, and cells were centrifuged and filtered with a 70-µm cell strainer.

Small intestines were harvested, and Peyer's patches were removed. They were then opened longitudinally and cut into small pieces. This was followed by treatment with HBSS containing 1 mM EDTA for 20 min at 37°C with constant stirring. After extensive washing, tissues were incubated with a digestion buffer (RPMI containing 2% newborn calf serum (Sigma), 20 µg/ml Liberase TH, and 10 U/ml DNase I) with continuous stirring at 37°C for 20 min. Supernatants were collected, and residual tissue pieces were digested again for 20 min. Supernatants from both digestions were combined and passed through 70-µm cell strainers to obtain single cells.

Dermal cells were prepared by splitting ears into dorsal and ventral halves with forceps and were treated with 0.25% trypsin in HBSS at 37°C for 1 h. They were then digested for 1 h at 37°C in RPMI containing 2% newborn calf serum, 80 µg/ml Liberase TH, and 10 U/ml DNase I. Single cells were collected after filtering digested tissues through a 70-µm cell strainer.

Flow cytometry and cell sorting

All antibodies used were purchased from BioLegend unless specified otherwise. The lineage (Lin) cocktail included anti-FcεR (MAR-1), anti-B220 (RA3-6B2), anti-CD19 (ID3), anti–Mac-1 (M1/70), anti–Gr-1 (R86-8C5), anti-CD11c (N418), anti-NK1.1 (PK136), anti–Ter-119 (Ter-119), anti-CD3ε (145-2C11), anti-CD5 (53-7.3), anti-CD8α (53-6.7), anti-TCRβ (H57-597), and anti-γδTCR (GL-3; eBioscience) unless specified otherwise. Additional antibodies are anti-CD45.2 (104), anti-CD45.1 (A20), anti-CD135 (A2F10), anti-cKit (2B8), anti-Sca-1 (D7), anti-Thy1.2 (53-2.1), anti–IL-5 (TRFK5), anti–IL-13 (eBio13A; eBioscience or Invitrogen), anti–IL-4 (11B11), anti–IL-17A (TC11-18H10.1), anti–IL-22 (IL22JOP; Invitrogen), anti-IFNγ (XMG1.2; eBioscience), anti–IL-7Rα (A7R34; eBioscience), anti-α4β7 (DATK32; eBioscience), anti-CD25 (PC61), anti–PD-1 (J43; eBioscience), anti-ST2 (DIH9), anti-ICOS (C398.4A), anti-DX5 (HMα2), anti-CD62L (MEL-14), anti-CD27 (LG.3A10), anti-CD122 (5H4; BD Biosciences), anti-siglecH (551), anti-MHCII (M5/114.152), anti-Sirpα (P84; eBioscience), anti-CD103 (2E7), anti-GATA3 (TWAJ; eBioscience), and anti-RORγt (Q31-376).

Cell sorting was performed on a FACSAria II (BD Biosciences). CLP, DN1, and DN3 cells were sorted as Lin$^-$IL-7R$^+$Sca-1^{int}ckit^{int}Thy1$^-$Flt3$^+$, Lin$^-$ST2$^-$cKit$^+$CD25$^-$, and Lin$^-$ST2$^-$cKit$^-$CD25$^+$, respectively. ILC2 cells were sorted as Lin$^-$TCRβ$^-$TCRγδ$^-$Thy1.2$^+$ST2$^+$ for thymus and BM and Lin$^-$TCRβ$^-$TCRγδ$^-$Thy1.2$^+$ST2$^+$ICOS$^+$ for lung. Lineage depletion were performed for thymus and BM cells before staining for specified lineage markers and antibodies for cell sorting as previously described (Perry et al., 2007). Briefly, purified antibodies were stained for BM lineage markers (B220, CD19, Ter119, Gr1, and Mac1) or thymus lineage markers (CD4 and CD8) followed by magnetic separation with BioMag anti-rat IgG beads (Qiagen). Flow cytometric analysis was performed on a LSR-II (BD Biosciences). Intracellular staining of transcription factors was performed using a Foxp3 Staining Buffer kit (eBioscience). Staining of cytokines was performed using a Cytofix/Cytoperm kit (BD Biosciences).

Gene rearrangement assay

Conventional PCRs were performed as described previously (Kim et al., 1999). Briefly, DNA was prepared at a concentration of 500 cells/µl by lysing cells in a digestion buffer (10 mM Tris, pH 8.4, 50 mM KCl, 2 mM $MgCl_2$, 0.45% NP-40, 0.45% Tween-20, and 60 µg/ml proteinase K), incubating at 55°C for 1 h, and then inactivating the protease at 95°C for 2 min. DNA equivalent to 1,000 genomes was used for PCR. Amplification products were detected by Southern blotting with radioactive labeled probes. Standard curves for PCR amplification were generated by using DNA samples made of mixtures of BM Mac1$^+$ cells and total thymocytes at different proportions. PCR products were analyzed in parallel with those generated from ILC2 samples in Southern blotting. Controls for DNA quantity were performed by PCR amplification of the ROSA26 locus. Primers for Dβ2-Jβ2, Vβ3-DJβ2, VαH-JαTT11, and Vγ1-Jγ4 rearrangement are as previously described (Capone et al., 1998; Kim et al., 1999). Primers for ROSA26 are 5′-GGAGTGTTGCAATACCTTTCTGG-3′ and 5′-CGACACTGTAATTTCATACTGTAG-3′. The probes for Vγ1-Jγ4 PCR products are 5′-CCCTTTGGCAAATATCTTGACCCATG-3′ and 5′-GCTGTGTTGGAGAAATATGGAAGAGAAAC-3′.

In vitro cell culture

Different progenitors were seeded in 48-well plates on OP9-DL1 stromal cells in α-MEM (Gibco) supplemented with 20% FBS, penicillin and streptomycin, β-mercaptoethanol, and glutamine (Sigma), as well as 30 ng/ml each of IL-2, IL-7, and stem cell factor (R&D Systems). The culture was split and replated onto fresh stromal layers after 7 d and then every 3–4 d. Cytokine production by ILC2s generated from the cultures was monitored after switching to a stroma-free condition supplemented with 10 ng/ml each of IL-2, IL-7, IL-25, and IL-33 for 3 d. To induce ERT2-Cre in vitro, 4-OHT was added into the cultures at a final concentration of 1 µM on day 4 after the initiation of the culture.

RNA-seq

RNA-seq was performed in duplicate by the Clinical Genomics Center at the Oklahoma Medical Research Foundation using the Ovation RNA-Seq System (NuGEN Technologies) followed by KAPA Hyper library preparation kits (KAPA Biosystems) on an Illumina NextSeq 500 sequencing platform with 76-bp, paired-end reads (Illumina). In addition, transcriptomes of WT DN3 thymocytes (Zhang et al., 2012) were included in our analyses. Raw sequencing reads (in a FASTQ format) were trimmed using Trimmomatic to remove any low-quality bases at the beginning or the end of sequencing reads as well as any adapter sequences (Bolger et al., 2014). Trimmed sequencing reads were aligned to the *Mus musculus* genome reference (GRCm38/mm10) using STAR v.2.4.0h (Dobin et al., 2013). Gene-level read counts were determined using HTSeq v.0.5.3p9 (Anders et al., 2015) with the GENCODE Release M10 (GRCm38) annotation. DESeq2 (Love et al., 2014) was used for read-count normalization and differentially expressed analyses of ILC2s isolated from Id1 transgenic and E protein–deficient mice. Only autosomal genes coding for lncRNAs, miRNAs, and protein-coding mRNAs were selected for analyses. Heatmaps were created by unsupervised hierarchical clustering using normalized read counts of differentially expressed transcripts (fold change >4, false discovery rate [FDR] < 0.0001) using the Morpheus program provided by the Broad Institute (https://software.broadinstitute.org/morpheus/). Volcano plots were generated using the R calibrate package (Graffelman, 2013). IPA (QiagenA) was used to analyze gene networks and pathways.

RNA-seq of cultured cells was performed in single strands. Read-count normalization and differentially expressed analyses was performed using the edgeR package from Bioconductor. Expression values normalized with the voom function were analyzed for differential expression using the standard functions of the limma program. A global score, quantifying expression variation among successive time points inside each cell type, was computed for each transcript using the *F* test, and the corresponding P values were adjusted for multiple testing using the FDR. The set of differentially expressed transcripts was segmented into six disjoint groups of similar expression variation profiles, using the HOPACH algorithm implemented in the R package of the same name. The HOPACH clustering algorithm builds a hierarchical tree by recursively partitioning a dataset while ordering and possibly collapsing clusters at each level. The mean/median split silhouette criterion is used to identify the level of the tree with maximally homogeneous clusters.

Data sharing

The RNA-seq data have been submitted to Gene Expression Omnibus with accession nos. GSE94597 and GSE111518.

Online supplemental material

Fig. S1 shows the dependence of the thymus on ILC2 production in Id1 transgenic mice and the appearance of tdTomato$^+$ ILC2s in the blood. Fig. S2 shows the post-sort analyses of samples used for TCR rearrangement assays and in vitro cultures. Fig. S3 shows the data of in vitro ILC2 culture initiated with DN3 cells from *plck*-Cre; HEB$^{f/f}$E2A$^{f/f}$ mice. Fig. S4 shows the analyses for ILC2 differentiation of cultured cells used for RNA-seq. Fig. S5 shows additional bioinformatics analyses of RNA-seq data.

Acknowledgments

We thank Dr. Avinash Bhandoola for suggestions and Dr. Yuan Zhuang for providing *plck*-Cre; E2A$^{f/+}$; HEB$^{f/+}$ mice. We thank Joni Kirwan, Benjamin Southard, Monica Davis, and Anna Bakowska for technical support. We are grateful to the Clinical Genomics Center, the Data Analysis Core and the Flow Cytometry facility at the Oklahoma Medical Research Foundation for outstanding technical assistance.

This work was supported by grants from the National Institutes of Health (1R01AI126851) and the Presbyterian Health Foundation to X.-H. Sun. X.-H. Sun holds the Lew and Myra Ward Chair in Biomedical Research at the Oklahoma Medical Research Foundation.

The authors declare no competing financial interests.

Author contributions: L. Qian performed most of the experiments with the help from S. Bajana and H.-C. Wang; C. Georgescu, V. Peng, and I. Adrianto carried out bioinformatics analyses; L. Qian, S. Bajana, and X.-H. Sun designed the study. L. Qian, J. Alberola-Ila, M. Colonna, J.D. Wren, and X.-H. Sun analyzed the data and wrote the manuscript.

Submitted: 13 November 2018
Revised: 24 January 2019
Accepted: 15 February 2019

References

Allende, M.L., J.L. Dreier, S. Mandala, and R.L. Proia. 2004. Expression of the sphingosine 1-phosphate receptor, S1P1, on T-cells controls thymic emigration. *J. Biol. Chem.* 279:15396–15401. https://doi.org/10.1074/jbc.M314291200

Anders, S., P.T. Pyl, and W. Huber. 2015. HTSeq–a Python framework to work with high-throughput sequencing data. *Bioinformatics.* 31:166–169. https://doi.org/10.1093/bioinformatics/btu638

Artis, D., and H. Spits. 2015. The biology of innate lymphoid cells. *Nature.* 517:293–301. https://doi.org/10.1038/nature14189

Bain, G., E.C. Maandag, D.J. Izon, D. Amsen, A.M. Kruisbeek, B.C. Weintraub, I. Krop, M.S. Schlissel, A.J. Feeney, M. van Roon, et al. 1994. E2A proteins are required for proper B cell development and initiation of immunoglobulin gene rearrangements. *Cell.* 79:885–892. https://doi.org/10.1016/0092-8674(94)90077-9

Bain, G., C.B. Cravatt, C. Loomans, J. Alberola-Ila, S.M. Hedrick, and C. Murre. 2001. Regulation of the helix-loop-helix proteins, E2A and Id3, by the Ras- ERK MAPK cascade. *Nat. Immunol.* 2:165–171. https://doi.org/10.1038/84273

Balciunaite, G., R. Ceredig, and A.G. Rolink. 2005. The earliest subpopulation of mouse thymocytes contains potent T, significant macrophage, and natural killer cell but no B-lymphocyte potential. *Blood.* 105:1930–1936. https://doi.org/10.1182/blood-2004-08-3087

Barndt, R.J., M. Dai, and Y. Zhuang. 2000. Functions of E2A-HEB heterodimers in T-cell development revealed by a dominant negative mutation of HEB. *Mol. Cell. Biol.* 20:6677–6685. https://doi.org/10.1128/MCB.20.18.6677-6685.2000

Bell, J.J., and A. Bhandoola. 2008. The earliest thymic progenitors for T cells possess myeloid lineage potential. *Nature.* 452:764–767. https://doi.org/10.1038/nature06840

Bolger, A.M., M. Lohse, and B. Usadel. 2014. Trimmomatic: a flexible trimmer for Illumina sequence data. *Bioinformatics.* 30:2114–2120. https://doi.org/10.1093/bioinformatics/btu170

Bornstein, C., S. Nevo, A. Giladi, N. Kadouri, M. Pouzolles, F. Gerbe, E. David, A. Machado, A. Chuprin, B. Toth, et al. 2018. Single-cell mapping of the

thymic stroma identifies IL-25-producing tuft epithelial cells. *Nature.* 559:622–626. https://doi.org/10.1038/s41586-018-0346-1

Capone, M., R.D. Hockett Jr., and A. Zlotnik. 1998. Kinetics of T cell receptor beta, gamma, and delta rearrangements during adult thymic development: T cell receptor rearrangements are present in CD44(+)CD25(+) Pro-T thymocytes. *Proc. Natl. Acad. Sci. USA.* 95:12522–12527. https://doi.org/10.1073/pnas.95.21.12522

Cisse, B., M.L. Caton, M. Lehner, T. Maeda, S. Scheu, R. Locksley, D. Holmberg, C. Zweier, N.S. den Hollander, S.G. Kant, et al. 2008. Transcription factor E2-2 is an essential and specific regulator of plasmacytoid dendritic cell development. *Cell.* 135:37–48. https://doi.org/10.1016/j.cell.2008.09.016

Cochrane, S.W., Y. Zhao, R.S. Welner, and X.H. Sun. 2009. Balance between Id and E proteins regulates myeloid-versus-lymphoid lineage decisions. *Blood.* 113:1016–1026. https://doi.org/10.1182/blood-2008-06-164996

Constantinides, M.G., B.D. McDonald, P.A. Verhoef, and A. Bendelac. 2014. A committed precursor to innate lymphoid cells. *Nature.* 508:397–401. https://doi.org/10.1038/nature13047

D'Cruz, L.M., M.H. Stradner, C.Y. Yang, and A.W. Goldrath. 2014. E and Id proteins influence invariant NKT cell sublineage differentiation and proliferation. *J. Immunol.* 192:2227–2236. https://doi.org/10.4049/jimmunol.1302904

Dias, S., R. Mansson, S. Gurbuxani, M. Sigvardsson, and B.L. Kee. 2008. E2A proteins promote development of lymphoid-primed multipotent progenitors. *Immunity.* 29:217–227. https://doi.org/10.1016/j.immuni.2008.05.015

Dobin, A., C.A. Davis, F. Schlesinger, J. Drenkow, C. Zaleski, S. Jha, P. Batut, M. Chaisson, and T.R. Gingeras. 2013. STAR: ultrafast universal RNA-seq aligner. *Bioinformatics.* 29:15–21. https://doi.org/10.1093/bioinformatics/bts635

Dudley, E.C., H.T. Petrie, L.M. Shah, M.J. Owen, and A.C. Hayday. 1994. T cell receptor beta chain gene rearrangement and selection during thymocyte development in adult mice. *Immunity.* 1:83–93. https://doi.org/10.1016/1074-7613(94)90102-3

Eberl, G., M. Colonna, J.P. Di Santo, and A.N. McKenzie. 2015. Innate lymphoid cells: A new paradigm in immunology. *Science.* 348:aaa6566. https://doi.org/10.1126/science.aaa6566

Gentek, R., J.M. Munneke, C. Helbig, B. Blom, M.D. Hazenberg, H. Spits, and D. Amsen. 2013. Modulation of Signal Strength Switches Notch from an Inducer of T Cells to an Inducer of ILC2. *Front. Immunol.* 4:334. https://doi.org/10.3389/fimmu.2013.00334

Graffelman, J. 2013. Calibrate: Calibration of Scatterplot and Biplot Axes. Package for drawing calibrated scales with tick marks on (non-orthogonal) variable vectors in scatterplots and biplots. Available at https://cran.r-project.org/web/packages/calibrate/index.html (accessed December 27, 2017).

Hoyler, T., C.S. Klose, A. Souabni, A. Turqueti-Neves, D. Pfeifer, E.L. Rawlins, D. Voehringer, M. Busslinger, and A. Diefenbach. 2012. The transcription factor GATA-3 controls cell fate and maintenance of type 2 innate lymphoid cells. *Immunity.* 37:634–648. https://doi.org/10.1016/j.immuni.2012.06.020

Huang, Y., K. Mao, X. Chen, M.A. Sun, T. Kawabe, W. Li, N. Usher, J. Zhu, J.F. Urban Jr., W.E. Paul, and R.N. Germain. 2018. S1P-dependent interorgan trafficking of group 2 innate lymphoid cells supports host defense. *Science.* 359:114–119. https://doi.org/10.1126/science.aam5809

Jones, R., E.J. Cosway, C. Willis, A.J. White, W.E. Jenkinson, H.J. Fehling, G. Anderson, and D.R. Withers. 2018. Dynamic changes in intrathymic ILC populations during murine neonatal development. *Eur. J. Immunol.* 48:1481–1491. https://doi.org/10.1002/eji.201847511

Kee, B.L. 2009. E and ID proteins branch out. *Nat. Rev. Immunol.* 9:175–184. https://doi.org/10.1038/nri2507

Kernfeld, E.M., R.M.J. Genga, K. Neherin, M.E. Magaletta, P. Xu, and R. Maehr. 2018. A Single-Cell Transcriptomic Atlas of Thymus Organogenesis Resolves Cell Types and Developmental Maturation. *Immunity.* 48:1258–1270. https://doi.org/10.1016/j.immuni.2018.04.015

Kim, D., X.C. Peng, and X.H. Sun. 1999. Massive apoptosis of thymocytes in T-cell-deficient Id1 transgenic mice. *Mol. Cell. Biol.* 19:8240–8253. https://doi.org/10.1128/MCB.19.12.8240

Klose, C.S., M. Flach, L. Mohle, L. Rogell, T. Hoyler, K. Ebert, C. Fabiunke, D. Pfeifer, V. Sexl, D. Fonseca-Pereira, et al. 2014. Differentiation of type 1 ILCs from a common progenitor to all helper-like innate lymphoid cell lineages. *Cell.* 157:340–356. https://doi.org/10.1016/j.cell.2014.03.030

Klose, C.S.N., T. Mahlakoiv, J.B. Moeller, L.C. Rankin, A.L. Flamar, H. Kabata, L.A. Monticelli, S. Moriyama, G.G. Putzel, N. Rakhilin, et al. 2017. The neuropeptide neuromedin U stimulates innate lymphoid cells and type 2 inflammation. *Nature.* 549:282–286. https://doi.org/10.1038/nature23676

Kondo, M., I.L. Weissman, and K. Akashi. 1997. Identification of clonogenic common lymphoid progenitors in mouse bone marrow. *Cell.* 91:661–672. https://doi.org/10.1016/S0092-8674(00)80453-5

Li, D., R. Guabiraba, A.G. Besnard, M. Komai-Koma, M.S. Jabir, L. Zhang, G.J. Graham, M. Kurowska-Stolarska, F.Y. Liew, C. McSharry, and D. Xu. 2014. IL-33 promotes ST2-dependent lung fibrosis by the induction of alternatively activated macrophages and innate lymphoid cells in mice. *J. Allergy Clin. Immunol.* 134:1422–1432. https://doi.org/10.1016/j.jaci.2014.05.011

Ling, F., B. Kang, and X.H. Sun. 2014. Id proteins: small molecules, mighty regulators. *Curr. Top. Dev. Biol.* 110:189–216. https://doi.org/10.1016/B978-0-12-405943-6.00005-1

Love, M.I., W. Huber, and S. Anders. 2014. Moderated estimation of fold change and dispersion for RNA-seq data with DESeq2. *Genome Biol.* 15:550. https://doi.org/10.1186/s13059-014-0550-8

Mao, A.P., M.G. Constantinides, R. Mathew, Z. Zuo, X. Chen, M.T. Weirauch, and A. Bendelac. 2016. Multiple layers of transcriptional regulation by PLZF in NKT-cell development. *Proc. Natl. Acad. Sci. USA.* 113:7602–7607. https://doi.org/10.1073/pnas.1601504113

Matloubian, M., C.G. Lo, G. Cinamon, M.J. Lesneski, Y. Xu, V. Brinkmann, M.L. Allende, R.L. Proia, and J.G. Cyster. 2004. Lymphocyte egress from thymus and peripheral lymphoid organs is dependent on S1P receptor 1. *Nature.* 427:355–360. https://doi.org/10.1038/nature02284

Miyazaki, M., K. Miyazaki, K. Chen, Y. Jin, J. Turner, A.J. Moore, R. Saito, K. Yoshida, S. Ogawa, H.R. Rodewald, et al. 2017. The E-Id Protein Axis Specifies Adaptive Lymphoid Cell Identity and Suppresses Thymic Innate Lymphoid Cell Development. *Immunity.* 46:818–834. https://doi.org/10.1016/j.immuni.2017.04.022

Mombaerts, P., A.R. Clarke, M.A. Rudnicki, J. Iacomini, S. Itohara, J.J. Lafaille, L. Wang, Y. Ichikawa, R. Jaenisch, and M.L. Hooper. 1992. Mutations in T-cell antigen receptor genes alpha and beta block thymocyte development at different stages. *Nature.* 360:225–231. https://doi.org/10.1038/360225a0

Murre, C. 2005. Helix-loop-helix proteins and lymphocyte development. *Nat. Immunol.* 6:1079–1086. https://doi.org/10.1038/ni1260

Nie, L., M. Xu, A. Vladimirova, and X.H. Sun. 2003. Notch-induced E2A ubiquitination and degradation are controlled by MAP kinase activities. *EMBO J.* 22:5780–5792. https://doi.org/10.1093/emboj/cdg567

Nussbaum, J.C., S.J. Van Dyken, J. von Moltke, L.E. Cheng, A. Mohapatra, A.B. Molofsky, E.E. Thornton, M.F. Krummel, A. Chawla, H.E. Liang, and R.M. Locksley. 2013. Type 2 innate lymphoid cells control eosinophil homeostasis. *Nature.* 502:245–248. https://doi.org/10.1038/nature12526

Perry, S.S., Y. Zhao, L. Nie, S.W. Cochrane, Z. Huang, and X.H. Sun. 2007. Id1, but not Id3, directs long-term repopulating hematopoietic stem-cell maintenance. *Blood.* 110:2351–2360. https://doi.org/10.1182/blood-2007-01-069914

Ricardo-Gonzalez, R.R., S.J. Van Dyken, C. Schneider, J. Lee, J.C. Nussbaum, H.E. Liang, D. Vaka, W.L. Eckalbar, A.B. Molofsky, D.J. Erle, and R.M. Locksley. 2018. Tissue signals imprint ILC2 identity with anticipatory function. *Nat. Immunol.* 19:1093–1099. https://doi.org/10.1038/s41590-018-0201-4

Robinette, M.L., and M. Colonna. 2016. Immune modules shared by innate lymphoid cells and T cells. *J. Allergy Clin. Immunol.* 138:1243–1251. https://doi.org/10.1016/j.jaci.2016.09.006

Sambandam, A., I. Maillard, V.P. Zediak, L. Xu, R.M. Gerstein, J.C. Aster, W.S. Pear, and A. Bhandoola. 2005. Notch signaling controls the generation and differentiation of early T lineage progenitors. *Nat. Immunol.* 6:663–670. https://doi.org/10.1038/ni1216

Schmitt, T.M., and J.C. Zuniga-Pflucker. 2002. Induction of T cell development from hematopoietic progenitor cells by delta-like-1 in vitro. *Immunity.* 17:749–756. https://doi.org/10.1016/S1074-7613(02)00474-0

Seillet, C., L.A. Mielke, D.B. Amann-Zalcenstein, S. Su, J. Gao, F.F. Almeida, W. Shi, M.E. Ritchie, S.H. Naik, N.D. Huntington, et al. 2016. Deciphering the Innate Lymphoid Cell Transcriptional Program. *Cell Reports.* 17:436–447. https://doi.org/10.1016/j.celrep.2016.09.025

Shi, J., and H.T. Petrie. 2012. Activation kinetics and off-target effects of thymus-initiated cre transgenes. *PLoS One.* 7:e46590. https://doi.org/10.1371/journal.pone.0046590

Sichien, D., C.L. Scott, L. Martens, M. Vanderkerken, G.S. Van, M. Plantinga, T. Joeris, P.S. De, L. Vanhoutte, M. Vanheerswynghels, et al. 2016. IRF8 Transcription Factor Controls Survival and Function of Terminally Differentiated Conventional and Plasmacytoid Dendritic Cells,

Respectively. *Immunity*. 45:626–640. https://doi.org/10.1016/j.immuni.2016.08.013

Spits, H., D. Artis, M. Colonna, A. Diefenbach, J.P. Di Santo, G. Eberl, S. Koyasu, R.M. Locksley, A.N. McKenzie, R.E. Mebius, et al. 2013. Innate lymphoid cells–a proposal for uniform nomenclature. *Nat. Rev. Immunol.* 13:145–149. https://doi.org/10.1038/nri3365

Sun, X.-H. 1994. Constitutive expression of the Id1 gene impairs mouse B cell development. *Cell.* 79:893–900. https://doi.org/10.1016/0092-8674(94)90078-7

Tait Wojno, E.D., and D. Artis. 2016. Emerging concepts and future challenges in innate lymphoid cell biology. *J. Exp. Med.* 213:2229–2248. https://doi.org/10.1084/jem.20160525

Vargas, C.L., J. Poursine-Laurent, L. Yang, and W.M. Yokoyama. 2011. Development of thymic NK cells from double negative 1 thymocyte precursors. *Blood.* 118:3570–3578. https://doi.org/10.1182/blood-2011-06-359679

Veinotte, L.L., C.P. Greenwood, N. Mohammadi, C.A. Parachoniak, and F. Takei. 2006. Expression of rearranged TCRgamma genes in natural killer cells suggests a minor thymus-dependent pathway of lineage commitment. *Blood.* 107:2673–2679. https://doi.org/10.1182/blood-2005-07-2797

Wallrapp, A., S.J. Riesenfeld, P.R. Burkett, R.E. Abdulnour, J. Nyman, D. Dionne, M. Hofree, M.S. Cuoco, C. Rodman, D. Farouq, et al. 2017. The neuropeptide NMU amplifies ILC2-driven allergic lung inflammation. *Nature.* 549:351–356. https://doi.org/10.1038/nature24029

Wang, H.C., S.S. Perry, and X.H. Sun. 2009. Id1 attenuates Notch signaling and impairs T-cell commitment by elevating Deltex1 expression. *Mol. Cell. Biol.* 29:4640–4652. https://doi.org/10.1128/MCB.00119-09

Wang, H.C., L. Qian, Y. Zhao, J. Mengarelli, I. Adrianto, C.G. Montgomery, J.F. Urban Jr., K.M. Fung, and X.H. Sun. 2017. Downregulation of E Protein Activity Augments an ILC2 Differentiation Program in the Thymus. *J. Immunol.* 198:3149–3156. https://doi.org/10.4049/jimmunol.1602009

Wojciechowski, J., A. Lai, M. Kondo, and Y. Zhuang. 2007. E2A and HEB are required to block thymocyte proliferation prior to pre-TCR expression. *J. Immunol.* 178:5717–5726. https://doi.org/10.4049/jimmunol.178.9.5717

Wong, S.H., J.A. Walker, H.E. Jolin, L.F. Drynan, E. Hams, A. Camelo, J.L. Barlow, D.R. Neill, V. Panova, U. Koch, et al. 2012. Transcription factor RORalpha is critical for nuocyte development. *Nat. Immunol.* 13:229–236. https://doi.org/10.1038/ni.2208

Xu, W., T. Carr, K. Ramirez, S. McGregor, M. Sigvardsson, and B.L. Kee. 2013. E2A transcription factors limit expression of Gata3 to facilitate T lymphocyte lineage commitment. *Blood.* 121:1534–1542. https://doi.org/10.1182/blood-2012-08-449447

Yagi, R., C. Zhong, D.L. Northrup, F. Yu, N. Bouladoux, S. Spencer, G. Hu, L. Barron, S. Sharma, T. Nakayama, et al. 2014. The transcription factor GATA3 is critical for the development of all IL-7Ralpha-expressing innate lymphoid cells. *Immunity.* 40:378–388. https://doi.org/10.1016/j.immuni.2014.01.012

Yang, Q., and A. Bhandoola. 2016. The development of adult innate lymphoid cells. *Curr. Opin. Immunol.* 39:114–120. https://doi.org/10.1016/j.coi.2016.01.006

Yang, Q., F. Li, C. Harly, S. Xing, L. Ye, X. Xia, H. Wang, X. Wang, S. Yu, X. Zhou, et al. 2015. TCF-1 upregulation identifies early innate lymphoid progenitors in the bone marrow. *Nat. Immunol.* 16:1044–1050. https://doi.org/10.1038/ni.3248

Yu, X., Y. Wang, M. Deng, Y. Li, K.A. Ruhn, C.C. Zhang, and L.V. Hooper. 2014. The basic leucine zipper transcription factor NFIL3 directs the development of a common innate lymphoid cell precursor. *eLife.* 3:e0446. https://doi.org/10.7554/eLife.04406

Yu, Y., J.C. Tsang, C. Wang, S. Clare, J. Wang, X. Chen, C. Brandt, L. Kane, L.S. Campos, L. Lu, et al. 2016. Single-cell RNA-seq identifies a PD-1hi ILC progenitor and defines its development pathway. *Nature.* 539:102–106. https://doi.org/10.1038/nature20105

Zhang, J.A., A. Mortazavi, B.A. Williams, B.J. Wold, and E.V. Rothenberg. 2012. Dynamic transformations of genome-wide epigenetic marking and transcriptional control establish T cell identity. *Cell.* 149:467–482. https://doi.org/10.1016/j.cell.2012.01.056

Zhiguang, X., C. Wei, R. Steven, D. Wei, Z. Wei, M. Rong, L. Zhanguo, and Z. Lianfeng. 2010. Over-expression of IL-33 leads to spontaneous pulmonary inflammation in mIL-33 transgenic mice. *Immunol. Lett.* 131:159–165. https://doi.org/10.1016/j.imlet.2010.04.005

Zhuang, Y., P. Soriano, and H. Weintraub. 1994. The helix-loop-helix gene E2A is required for B cell formation. *Cell.* 79:875–884. https://doi.org/10.1016/0092-8674(94)90076-0

Zook, E.C., and B.L. Kee. 2016. Development of innate lymphoid cells. *Nat. Immunol.* 17:775–782. https://doi.org/10.1038/ni.3481